AB INITIO INVESTIGATIONS ON ELECTRONIC AND LATTICE DYNAMICAL PROPERTIES OF INTERCALATION OF METALS INTO HEXAGONAL BORON NITRIDE

by

BAHADIR ALTINTAŞ

THESIS SUBMITTED TO
THE GRADUATE SCHOOL OF NATURAL AND APPLIED SCIENCES
OF
THE ABANT İZZET BAYSAL UNIVERSITY
IN PARTIAL FULFILLMENT OF THE REQUIREMENTS FOR THE DEGREE
OF
DOCTOR OF PHILOSOPHY
IN
THE DEPARTMENT OF CHEMISTRY

JULY 2009

Approval of the Graduate School of Natural Sciences

Prof. Dr. Nihat Çelebi

Director

I certify that this thesis satisfies all the requirements as a thesis for the degree of Doctor of Philosophy.

Prof. Dr. Çetin Bozkurt

Head of Chemistry Department

This is to certify that we have read this thesis and that in our opinion it is fully adequate, in scope and quality as a thesis for the degree of Doctor of Philosophy.

Prof.Dr.Çetin Bozkurt
Supervisor

Assoc.Prof.Dr.Resul Eryiğit
Co-supervisor

Examining Committee Members

1. Prof. Dr. İbrahim Belenli ..... İ.Belenli .....
2. Prof. Dr.Çetin Bozkurt .....
3. Assoc. Prof. Dr. Resul Eryiğit .....
4. Prof. Dr. Canan Ünaleroğlu .....
5. Assoc. Prof. Dr. Engin Özdaş .....

ABSTRACT

AB INITIO INVESTIGATIONS ON ELECTRONIC AND LATTICE DYNAMICAL PROPERTIES OF INTERCALATION OF METALS INTO HEXAGONAL BORON NITRIDE

Altıntaş, Bahadır

Ph.D., Department of Chemistry

Supervisor: Prof. Dr. Çetin Bozkurt

Co-Supervisor: Assoc. Prof. Dr. Resul Eryiğit

July 2009, 105 pages

Although hexagonal boron nitride(hBN) is quite similar to graphite structurally, it has been very difficult to obtain any intercalation compound of hBN while there are hundreds of graphite intercalation compounds. We have investigated the possible intercalation of hBN by alkali atoms in the density functional theory framework by using pseudopotentials and plane-wave basis. The structural, electronic and lattice dynamical properties of hypothetical hBN analogues of C_3Li, C_6Li, C_6Ca,$(BN)_3Li$, $(BN)_6Li_4$, $(BN)_3Ca$ and copper intercalated $(BN)_3Cu$ are calculated.We have found that although the electronic structure, band structure and fermi surface of alkali intercalated hBN is very similar to that of alkali intercalated graphite, the lattice dynamics show a set of negative

frequency modes which indicate that alkali-intercalated hBN is not stable. Also there were no problem in structural and electronical structure calculations of Cu intercalated hBN but, Γ point phnon calculations gives negative frequencies which indicates the structure is metastable.

Keywords: Boron nitride,intercalation, graphite intercalation compounds, density functional theory, lattice dynamics, electronic structure

ÖZET

HEKZAGONAL BOR NİTRÜR METAL İNTERKALASYON BİLEŞİKLERİNİN ELEKTRONİK VE ÖRGÜ DİNAMİK ÖZELLİKLERİNİN AB INITO YÖNTEMLE İNCELENMESİ

Altıntaş, Bahadır

Doktora, Kimya Bölümü

Tez Danışmanı: Prof. Dr. Çetin Bozkurt

Yardımcı Tez Danışmanı: Doç. Dr. Resul Eryiğit

Temmuz 2009, 105 sayfa

Hekzagonal bor nitrür(hBN) grafite çok benzer bir yapıya sahip olmasına rağmen, grafitin yüzlerce interkalasyon bileşiği bulunurken hBN interkalasyon bileşiği elde etmek çok zordur. Bu çalışmada mümkün olabilecek hBN interkalasyon bileşiklerini yoğunluk fonksiyonu teorisi çerçevesinde yalancı potansiyeller ve düzlem dalga taban kullanarak incelemeye çalıştık. Hexagonal bor nitrürürn C_3Li, C_6Li ve C_6Ca benzerleri olan $(BN)_3Li$,$(BN)_6Li_4$,$(BN)_3Li$ ve bakır intecalasyon bileşiği olan $(BN)_3Cu$ için yapısal, elektronik ve örgü dinamiği özellikleri hesaplandı. hBN alkali interkalasyon bileşiklerinin elektronik yapı, bant yapısı ve fermi yüzeyleri grafit alkali interkalasyon bileşikleri benzerlerine oldukça yakın sonuçlar verdi. Örgü dinamiği hesaplamaları ise alkali-hBN interkalasyon bileşiklerinin kararlı olmadığını gösteren negatif frekanslar gösterdi. Hekzagonal bor nitrürün bakır

interkalasyon bileşiği için de yapısal ve elektronik olarak hesaplamalarda sorun görülmezken, tek nokta fonon hesaplamaları bu yapının kararsız olduğunu gösteren negatif frekanslar verdi.

Anahtar Kelimeler: Bor nitrür,interkalasyon, grafit interkalasyon bileşikleri, yoğunluk fonksiyonu teorisi, örgü dinamiği, elektronik yapı

..to My Family and Friends

ACKNOWLEDGEMENTS

I should convey my heartfelt gratitude to everyone who helped me in the preparation and completion of this thesis.

I owe a great deal to my supervisor, Assoc.Prof.Dr. Resul Eryiğit and Prof. Dr. Çetin Bozkurt for moral support, guidance and supervision throughout this study. Their assistance brought my thesis to completion.

I am also thankful to my dear colleagues for their invaluable contributions.

I would also express my gratitude to Dr.Cihan Parlak for his support and patience throughout this study.

TABLE OF CONTENTS

LIST OF TABLES

LIST OF FIGURES

CHAPTER 1

INTRODUCTION

Hexagonal boron nitride(hBN) is isoelectronic to graphite and their lattice structures are quiet similar. The main difference between them is in terms of their electronic structure, while graphite is semi-metal, hBN is a wide gap semiconductor. Intercalation of graphite with electron donor or acceptor atom or molecules leads to compounds with desirable optical, electronic and structural properties. Graphite intercalation which involves atoms residing in between the carbon sheets proved to be quiet easy and hundreds of graphite intercalation compounds have been synthesized over the last 50 years, while intercalating hBN with any atom or functional group proved to be extremely difficult and no successful hBN intercalation compound has been reported so far.

The aim of the present thesis is to investigate the intercalation of hBN with alkali(Li), earth-alkali (Ca) and transition metal (Cu) atoms by using quantum mechanical first principles calculations. The chosen approach is the so called Density Functional Theory which uses electronic density as the basic quantity to calculate the properties of a collection of atoms.

As the basis for comparisons for the results obtained we have also investigated the graphite intercalation compounds of the same intercalants. Within the context of the thesis, we have calculated following quantities:

For copper intercalation we have considered a low copper concentration $(BN)_{32}Cu$ intercalation and found that the copper tends to form electronic bond as a bridge between B and N atoms. The lattice dynamical studies indicate that this compound is metastable and would not last long.

For lithium intercalation, we have investigated a large number of properties; first of all we have analyzed the equilibrium structure of the Li-intercalated graphite and hBN and found theory was reasonably good in predicting the experimentally observed structure. This finding is support for the predicted Li-intercalated hBN structure. In intercalation of graphite with alkali atoms, an important question that has been controversial for the last 30 years was the magnitude of charge transfer from the intercalant to the graphite layers. Some experiments and theoretical studies indicate a full transfer of alkali s electron to the carbon layers, while others indicate negligible or very small charge transfer. Also, the observance of superconductivity in C_6Ca at relatively high 11.5 ^oK has been explained by the role of the amount of the charge transfer. We have calculated the charge transfer for lithium intercalation into hBN and graphite and found transferred 0.2 e^- charge to be which supports the experiments that report low charge transfer.

For the lithium intercalation, we have also calculated the electronic structure such as band structure, total electronic density of states and fermi surface of the intercalated compounds and found important similarities between graphite and hBN intercalation compounds. Both lattice dynamical calculations and formation enthalpy calculations indicate that Li intercalated compounds can only be obtained under high pressure and could be unstable.

We also have investigated the intercalation of graphite and hBN with earth-alkaline calcium. The similarities in electronic structure of both intercalation compounds indicate that $(BN)_3Ca$ can also be superconducting as indicated by occupied interlayer states and a high density of states at the fermi level. But again, lattice dynamics indicate that this compound is also unstable.

The outline of the thesis is as follows: In Chapter 2 a brief review of density

functional theory is given, density functional perturbation theory, which is used to calculate the lattice dynamical properties is reviewed in Chapter 3. The copper intercalation study is presented in Chapter 4, while Chapter 5 and 6 is about the first principles investigation of lithium intercalation of graphite and hBN, Chapter 7 presents the results of calcium intercalation into graphite and hBN.

CHAPTER 2

DENSITY FUNCTIONAL THEORY

Quantum mechanically, a crystal can be considered as a system where electrons and nuclei interact through coulombic(electrostatic) forces. Due to greater mass of nuclei when compared with electrons, the motion of nuclei is much slower than that associated electrons. Entangling of nuclear degree of freedom is referred to as "adiabatic approximation" (or Born-Oppenheimer approximation).

The problem can be divided into two parts. The first part is the problem of electrons as if the nuclei are not moving and the second part of the problem is the problem of nuclei moving on a potential surface that described by electronic distribution.

The electronic energy band structure and electronic wave functions of the crystal can be obtained from the solution of the first problem, while the vibrational properties of the crystal can be obtained from the solution of the second problem.

If we start with the first problem, consider that we have N electrons interacting in an external potential which created by stationary nuclei. Quantum mechanically, this system can be described by Schrödinger many body equation

$$H\psi(\vec{r}_1, ..., \vec{r}_N) = E\psi(\vec{r}_1, ..., \vec{r}_N) \tag{2.1}$$

where H in the Hamiltonian:

$$H = -\frac{1}{2m_e}\sum_{i=1}^{N}\nabla_i^2 - \sum_{i=1}^{N}V_{ext}(\vec{r}_i) + \frac{e^2}{2}\sum_{i\neq j}\frac{1}{|\vec{r}_i - \vec{r}_j|} \tag{2.2}$$

where $\vec{r_i}$ is the position of the i^{th} electron and $V_{ext}(\vec{r_i})$ is the external potential that act on the electron i. In these formulas we are using atomic units, where $\hbar = 1$; if $m_e = \frac{1}{2}$ and $e^2 = 2$ then the energies are in Rydberg (Ryd) or if $m_e = 1$, $e^2 = 1$, energies are in Hartree (Ha).

In practice, the solution of Equation (2.1) cannot be found analytically or numerically in full quantum-mechanical framework, because coulombic form couples all the electronic degrees of freedom. To overcome this problem, its convenient to find the ground-state charge density, which can also be used to calculate the observable ground-state properties of the crystal instead of to find many-body wave-function which solve Equation (2.1).

Practically, Equation (2.2) is replaced by equation derived from density functional theory (DFT) of Hohenberg and Kohn [1]. This theory shows that the external potential acting on electrons is a functional of the ground-state charge density. This potential, in turn, determines the ground-state wave-function and therefore all the ground-state properties of the electronic system are uniquely determined by its ground-state charge density distribution.

An important ground-state observable is the total energy of the system. Charge density can be found as the function that minimizes the total energy functional as demonstrated by Kohn and Sham (KS) [2].

Formally, one can write the ground-state energy of the many-body system as the expectation value of the Hamiltonian as;

$$G[n] =< \psi_0|H|\psi_0 > \tag{2.3}$$

Let us specialize the situation to properties of periodic solids, where nuclear position are fixed by the introduction of Bravais lattice vectors K_μ, and by the choice of basis vectors τ_s which characterize the positions of the nuclei inside the

unit cell so that the total energy of the electrons and the nuclei can be written as;

$$E_{tot} = E_{i-i} + G[n] \tag{2.4}$$

where E_{i-i} , the coulombic potential energy of the ionic subsystem which can be computed as;

$$E_{i-i} = \frac{e^2}{2} \sum_{\mu\nu}{}' \sum_{ss_1} \frac{Z_s Z_{s_1}}{|R_\mu + \tau_s - R_\nu - \tau_{s_1}|} \tag{2.5}$$

where Z_s, the charge of nucleus at τ_s and prime on summation indicates that $\mu = \nu$ and $s = s_1$ term is omitted from the sum.

Kohn and Sham introduced a new functional $G[n]$ with help of wave-functions of independent electron gas with the same density as the interacting system.

Within this approach, let $|\psi_i>$ be the single particle wave functions of non-interacting system, then the kinetic energy would be

$$T = -\frac{1}{2m_e} \sum_i f_i < \psi_i|\nabla^2|\psi_i > \tag{2.6}$$

where f_i is the Fermi function, which is equal to 2 (taking into account spin degeneracy) if the energy of the i^{th} level is less than Fermi energy and equals 0 if it is higher. The density of same non-interacting system would be;

$$n(\vec{r}) = \sum_i f_i |\psi_i(\vec{r})|^2 \tag{2.7}$$

this density, by construction, is same as the density of the interacting system. So E_{tot} would include a coulombic term of the form;

$$E_H = \frac{e^2}{2} \int_V \int_V d\vec{r}_2 d\vec{r}_1 \frac{n(\vec{r}_2)n(\vec{r}_1)}{|\vec{r}_1 - \vec{r}_2|} \tag{2.8}$$

External interaction would give;

$$E_{ext} = \sum_i f_i < \psi_i | V_{ext} | \psi_i > \tag{2.9}$$

In practice V_{ext} is the effect of nuclei. If these terms are extracted from the total energy of the interacting system one would get a functional that includes all the many-particle effects. This part of the total energy is known as the exchange-correlation energy of the system

$$E_{xc}[n] = G[n] - E_{ext} - T - E_H \tag{2.10}$$

If $E_{xc}[n]$ was known, the ground state density could be computed by minimizing total ground state energy. This minimization is alone with respect to single-particle wave function $\psi_i(r)$ with the orthogonality constraint;

$$< \psi_i | \psi_j >= \delta_{ij} \tag{2.11}$$

which leads to Kohn-Sham equations;

$$\left[-\frac{1}{2m_e} \nabla^2 + V_H(\vec{r}) + V_{xc}(\vec{r}) + V_{ext}(\vec{r}) \right] \psi_i(\vec{r}) = \epsilon_{ij} \psi_i(\vec{r}) \tag{2.12}$$

The solutions of this equation are used to build up charge density $n(\vec{r})$ in Equation (2.7) in Equation (2.12);

$$V_H(\vec{r}) = e^2 \int_V d\vec{r_1} \frac{n(\vec{r}_1)}{|\vec{r} - \vec{r}_1|} \tag{2.13}$$

and

$$V_{xc}(\vec{r}) = \frac{\delta E_{xc}[n]}{\delta n(\vec{r})} \tag{2.14}$$

The physical observable of KS are total ground-state energy and ground-state charge density.

2.1 The Plane-Wave Pseudopotential Method

In a periodic system, Equation (2.12) can be solved by expanding $\psi_i(\vec{r})$ in a complete set of basis functions, such as plane waves (PW), gaussian functions or atomic orbitals. We will use only the plane wave expansion because of its features as simple to use and computational advantages. Because of lattice periodicity, plane waves are natural basis and they don't suffer from basis towards atomic positions. Hartree potential is easier to compute with PW, and one can systematically increase the resolution of the computation by increasing the number of plane waves used to expand $\psi_i(\vec{r})$.

Since $V_{ext}(\vec{r})$ is the nuclear potential, the wave functions if electrons close to nuclei would have highly oscillatory structure, which can be described only huge number of plane waves to get enough acceptable resolutions. From our knowledge, the electrons that important in bonding are valance electrons. And the energies associated with core wave functions are orders of magnitude higher than the energies associated with the valance wave functions. In this case one can eliminated the core electrons which are tightly bond to the nuclei, from Equation (2.12); then can use valance electrons only instead of the all-electrons as a equivalent cases.

This approximation amounts to substitution of nuclear potential with a pseudopotential whose lowest energies coincides with the valence all-electron energies and whose wave-functions coincide with all-electron wave functions in regions far

away from the nucleus.

Pseudopotential theory has been developed to great accuracies in last three decades. In practice, the pseudopotential of nuclei s is written as

$$V_s(\vec{r}) = V_s^{loc}(\vec{r}) + \sum_{i=0}^{l_{max}} V_{s,l}^{nl}(\vec{r}) P_l \tag{2.15}$$

where P_l is the projector

$$P_l f(\vec{r}) = \sum_{m=-l}^{l} f_{lm}(\vec{r}) Y_l^m(\theta, \phi) \tag{2.16}$$

where Y_l^m is the spherical harmonic of singular momentum l and f_{lm} are the expansion coefficients the function $f(\vec{r})$.

2.2 Plane-Wave Solution of Kohn-Sham Equations

Equation (2.12) is a nonlinear differential eigenvalue equation. The plane wave solutions of this equation for a periodic solid with volume V were given in [3]

Define the KS potential as

$$V_{KS}(\vec{r}) = V_{ext}(\vec{r}) + V_H(\vec{r}) + V_{xc}(\vec{r}) \tag{2.17}$$

this potential will be periodic with the periodicity of the Bravais lattice as;

$$V_{KS}(\vec{r} + \vec{R}_\mu) = V_{KS}(\vec{r}) \tag{2.18}$$

so we can apply Bloch's theorem [4] to Equation (2.12) :

$$\psi_i(\vec{r}) = \psi_i(\vec{k}, \vec{r}) = e^{i\vec{k}\cdot\vec{r}} u_i(\vec{k}, \vec{r}) \tag{2.19}$$

where $\vec{k}$ is a vector inside 1^{st} Brillouin zone and $u_i(\vec{k}, \vec{r})$ periodic with the peri-

odicity of the direct lattice:

$$u_i(\vec{k}, \vec{r} + \vec{R}_\mu) = u_i(\vec{k}, \vec{r}) \tag{2.20}$$

If we have N electrons, we would need $\frac{N}{2}$ lowest filled states factor 2 from $\vec{k}$-points inside the 1^{st} Brillouin zone depends on the boundary conditions and it is equal to number of cells in the case of periodic boundary conditions. So number of full bands, N_b, to one half the number of electrons is the unit cell.

If we insert Equation (2.19) into Equation (2.12) we obtain:

$$\left[\frac{1}{2m_e}(-i\nabla + \vec{k})^2 + V_H(\vec{r}) + V_{xc}(\vec{r}) + V_{ext}(\vec{k}, \vec{r})\right] u_i(\vec{k}, \vec{r}) = \epsilon_i(\vec{k}) u_i(\vec{k}, \vec{r}) \tag{2.21}$$

where

$$V_{ext}(\vec{k}, \vec{r}) = e^{-i\vec{k}\cdot\vec{r}} V_{ext}(\vec{r}) e^{i\vec{k}\cdot\vec{r}} \tag{2.22}$$

Equation (2.21) are N_c different equations (N_c is the number of cells of the crystal). Each of these equations can be solved more easily than original Equation (2.12), because $u_i(\vec{k}, \vec{r})$ have the periodicity of the Bravais lattice and it is possible to expand it in plane waves as;

$$u_i(\vec{k}, \vec{r}) = \frac{1}{\sqrt{V}} \sum_G C_{\vec{k}+\vec{G},i} e^{i\vec{G}\cdot\vec{r}} \tag{2.23}$$

where $\vec{G}$ is a reciprocal vector and $C_{\vec{k}+\vec{G},i}$ are the eigenvectors of a linear eigenvalue problem, obtained by inserting Equation (2.23) into Equation (2.21) as;

$$\sum_{\vec{G}_1}\left[\frac{1}{2m_e}|\vec{k}+\vec{G}|^2\delta_{\vec{G},\vec{G}_1}+V_H(\vec{G}-\vec{G}_1)+V_{xc}(\vec{G}-\vec{G}_1)+V_{ext}(\vec{k}+\vec{G},\vec{k}+\vec{G}_1)\right]C_{\vec{k}+\vec{G}_1,i} \quad = \\ = \epsilon_i(\vec{k})C_{\vec{k}+\vec{G},i} \quad (2.24)$$

where

$$n_V(\vec{G}) = \frac{1}{\Omega}\int_\Omega d\vec{r} n_V(\vec{r})e^{-i\vec{G}\cdot\vec{r}} \quad (2.25)$$

and

$$V_H(\vec{G}) = 4\pi e^2\frac{n_V(\vec{G})}{|\vec{G}^2|} \quad (2.26)$$

and $V_{xc}(\vec{G})$ is the Fourier transform of exchange-correlation potential; Ω is the volume of unit cell. The external potential term is;

$$V_{ext}(\vec{k}+\vec{G},\vec{k}+\vec{G}_1) = \frac{1}{V}\int_V d\vec{r}e^{-i\vec{G}\cdot\vec{r}}V_{ext}(\vec{k},\vec{r})e^{i\vec{G}_1\cdot\vec{r}} \quad (2.27)$$

The practical solution of Equation (2.24) involves a finite basis set. For pseudopotentials the size of basis is determined by the structure of V_{ext}.

Equation(2.24) is an eigenvalue problem and can be solved by standard numerical methods [5] if the number of G vectors in the expansion is low enough. The traditional eigenvalue methods requires N^3 operations [5]. Even for a small system with 1000 plane-waves, the diagonalization process would be 10^9 operations. Furthermore, only the first very few of the eigenvalues and eigenvectors are relevant for most of the calculations. Based on this observations there has been many different attempts to develop iterative algorithms that would depend on N with a power less than 3. The method used in the calculations reported in

this study is direct minimization of the Kohn-Sham total energy functional with a conjugate gradient algorithm. The details of this approach in beyond the scope of this thesis and can be found in [6].

CHAPTER 3

DENSITY FUNCTIONAL PERTURBATION THEORY

3.1 Overview

Ground-state properties of a periodic system discussed in previous chapter in the framework of density functional theory. Ground-state properties of a system can give many information about the physical statements of a system such as total energy, lattice constants, charge density and bulk modulus. Other physical properties which are accessible experimentally are related to the reaction of the system against the application of external perturbations such as small atomic displacements, strain perturbations and macroscopic electric fields. These perturbations have a particular importance and are the main interest of this work. Most of the physical properties are related to the second derivatives of total energy of the system after these perturbations applied. For example, the force used on a nuclei is related to the first derivative of the energy with respect to atomic displacements and the first derivative of the energy with respect to homogeneous electric field gives the dipole moment of a molecule. Many other physical quantities such as dielectric tensor, Born effective charge tensors, elastic constants and phonon dispersion spectra are related to the first derivatives of the total energy of the system.

Two methods are exist for determination of the properties above. The first method is the direct-method which is also known as *frozen-phonon technique*[7]. By this method, total energy of unperturbed and perturbed system and energy derivatives can be determined numerically. Then one can construct the dynamical

matrix to obtain phonon frequencies. The practical advantage of this method is requirement of simple ground-state calculations. But this method can not handle perturbations with periodic lattice. It is also impossible to obtain quantities of the system under the homogeneous electric field because of its linear potential in space. If calculation of the phonon frequencies away from the Brillouin zone center ($\mathbf{q} \neq \mathbf{0}$) is attempted within the frozen-phonon approach, supercells must be used, but this increases the computing time.

The second method is the use of the perturbation theory to evaluate the response functions directly within the density functional framework. There are two formalism for this perturbative approach. In the Baroni, Giannozzi and Testa (BGT) formalism [8, 9], a series of equations, so-called Sternheimer equations, are obtained and the solution can be done self-consistently to calculate linear responses. Gonze formalism [10, 11, 12, 13] is basically the consideration of the perturbation theory applied to a variational principle. This method says that the minimization of a variational expression of second-order energy derivatives can be used to derive first-order wave-functions. Both of these two methods allow us to calculate dispersion of phonons at any wave-vector and do not require supercells which increases the computing time. These methods are, in the linear-response theory, in the framework DFT, referred as *density functional perturbation theory* (DFPT).

3.2 Basics of Perturbation Theory

In the DFT chapter, we have discussed the formulation of DFT and calculation of ground state properties of a periodic solid without perturbation. so we assume that all the ground-state properties such as total energy, wave functions and charge density of the system are known. to obtain the derivatives of the total

energy of the system with respect to an applied perturbation obtained by the parameter λ, the new problem is described with Schrödinger equation as:

$$H(\lambda)|\psi_n(\lambda)\rangle = E(\lambda)|\psi(\lambda)\rangle. \tag{3.1}$$

The external potential v_{ext} that depend on the parameter λ, can be expanded to a Taylor series and it is supposed to be known to all orders:

$$v_{\text{ext}}(\lambda) = v_{\text{ext}}^{(0)} + \lambda v_{\text{ext}}^{(1)} + \lambda^2 v_{\text{ext}}^{(2)} + \dots \tag{3.2}$$

Since we are interested the changes of physical quantities (total energy, wave-functions, electronic charge density or Hamiltonian) due to the perturbation of the external potential (Eqn. 3.2) these perturbed quantities $X(\lambda)$ can be expanded with the same form of $v_{\text{ext}}(\lambda)$,

$$X(\lambda) = X^{(0)} + \lambda X^{(1)} + \lambda^2 X^{(2)} + \dots \tag{3.3}$$

Let us consider the hamiltonian $H(\lambda)$ in Eqn. 3.1 is supposed to be known in the first-order:

$$H(\lambda) = H^{(0)} + \lambda H^{(1)} \tag{3.4}$$

and writing wave function $\psi_n(\lambda)$ and energy $\varepsilon_n(\lambda)$ as power series like Eqn. 3.3, respectively;

$$\psi_n(\lambda) = \psi_n^{(0)} + \lambda \psi_n^{(1)} + \lambda^2 \psi_n^{(2)} + \dots \tag{3.5}$$

and

$$\varepsilon_n(\lambda) = \varepsilon_n^{(0)} + \lambda \varepsilon_n^{(1)} + \lambda^2 \varepsilon_n^{(2)} + \dots \tag{3.6}$$

Inserting Eqns. 3.4, 3.5, and 3.6 to Eqn. 3.1 we get:

$$H^{(0)}\left|\psi_n^{(0)}\right\rangle + \lambda\left(H^{(1)}\left|\psi_n^{(0)}\right\rangle + H^{(0)}\left|\psi_n^{(1)}\right\rangle\right) + \lambda^2\left(H^{(1)}\left|\psi_n^{(1)}\right\rangle + H^{(0)}\left|\psi_n^{(2)}\right\rangle\right) + \ldots$$
$$= \varepsilon_n^{(0)}\left|\psi_n^{(0)}\right\rangle + \lambda\left(\varepsilon_n^{(1)}\left|\psi_n^{(0)}\right\rangle + \varepsilon_n^{(0)}\left|\psi_n^{(1)}\right\rangle\right) + \lambda^2\left(\varepsilon_n^{(2)}\left|\psi_n^{(0)}\right\rangle + \varepsilon_n^{(1)}\left|\psi_n^{(1)}\right\rangle + \varepsilon_n^{(0)}\left|\psi_n^{(2)}\right\rangle\right) + \ldots \quad (3.7)$$

If we take $\lambda = 0$ in Eqn. 3.7 we get the unperturbed equation:

$$H^{(0)}\left|\psi_n^{(0)}\right\rangle = \varepsilon^{(0)}\left|\psi_n^{(0)}\right\rangle \quad (3.8)$$

with no surprise and supposed to be calculated from DFT described in previous chapter. Derivation of Eqn. 3.7 with respect to λ and then taking $\lambda = 0$ we get first-order perturbation of Schrödinger equation;

$$H^{(1)}\left|\psi_n^{(0)}\right\rangle + H^{(0)}\left|\psi_n^{(1)}\right\rangle = \varepsilon_n^{(1)}\left|\psi_n^{(0)}\right\rangle + \varepsilon_n^{(0)}\left|\psi_n^{(1)}\right\rangle \quad (3.9)$$

and if we differentiate Eqn. 3.7 with respect to λ two times and then take $\lambda = 0$ we get second-order of perturbation:

$$H^{(1)}\left|\psi_n^{(1)}\right\rangle + H^{(0)}\left|\psi_n^{(2)}\right\rangle = \varepsilon_n^{(2)}\left|\psi_n^{(0)}\right\rangle + \varepsilon_n^{(1)}\left|\psi_n^{(1)}\right\rangle + \varepsilon_n^{(0)}\left|\psi_n^{(2)}\right\rangle. \quad (3.10)$$

To obtain first derivative of the energy $\varepsilon_n^{(1)}$ we can premultiplicate Eqn. 3.9 by $\left\langle\psi_n^{(0)}\right|$,

$$\left\langle\psi_n^{(0)}\right| H^{(1)}\left|\psi_n^{(0)}\right\rangle + \left\langle\psi_n^{(0)}\right| H^{(0)}\left|\psi_n^{(1)}\right\rangle = \varepsilon_n^{(1)}\left\langle\psi_n^{(0)}|\psi_n^{(0)}\right\rangle + \varepsilon_n^{(0)}\left\langle\psi_n^{(0)}|\psi_n^{(1)}\right\rangle. \quad (3.11)$$

Since $H^{(0)}$ is hermitian, it is possible to write

$$\left\langle\psi_n^{(0)}\right| H^{(0)}\left|\psi_n^{(1)}\right\rangle = \left\langle\psi_n^{(0)}\right| \varepsilon_n^{(0)}\left|\psi_n^{(1)}\right\rangle = \varepsilon_n^{(0)}\left\langle\psi_n^{(0)}|\psi_n^{(1)}\right\rangle \quad (3.12)$$

and using $\left\langle \psi_n^{(0)} | \psi_n^{(0)} \right\rangle = 1$, from Eqn. 3.11, we obtain the equation for first-order energy :

$$\varepsilon_n^{(1)} = \left\langle \psi_n^{(0)} \right| H^{(1)} \left| \psi_n^{(0)} \right\rangle . \tag{3.13}$$

This is the fundamental result of first-order perturbation theory. in order to obtain the first derivative of the energy the knowledge of the unperturbed ground-state wave functions of the system and the perturbation hamiltonian $H^{(1)}$ are needed while to calculate first-order wave functions $\psi_n^{(1)}$ are not.

To obtain the second derivative of the energy, starting from second-order Schrödinger equation (3.10) we premultiplicate by $\left\langle \psi_n^{(0)} \right|$ and get

$$\varepsilon_n^{(2)} = \left\langle \psi_n^{(0)} \right| H^{(1)} - \varepsilon_n^{(1)} \left| \psi_n^{(1)} \right\rangle \tag{3.14}$$

where we have used the relation

$$\left\langle \psi_n^{(0)} \right| H^{(0)} \left| \psi_n^{(2)} \right\rangle = \left\langle \psi_n^{(0)} \right| \varepsilon_n^{(0)} \left| \psi_n^{(2)} \right\rangle . \tag{3.15}$$

At this point, we do need the first-order wave functions $\psi_n^{(1)}$ to get second-order energy derivative $\varepsilon_n^{(2)}$.

The first-order wave functions $\psi_n^{(1)}$ are generally expanded in terms of a sum over unperturbed wave functions[14, 15],

$$\left| \psi_n^{(1)} \right\rangle = \sum_{m \neq n} C_{mn}^{(1)} \left| \psi_m^{(0)} \right\rangle \tag{3.16}$$

where the expansion coefficient $C_{mn}^{(1)}$ is given by

$$C_{mn}^{(1)} = \frac{\left\langle \psi_m^{(0)} \right| H^{(1)} \left| \psi_n^{(0)} \right\rangle}{\varepsilon_n^{(0)} - \varepsilon_m^{(0)}}. \tag{3.17}$$

The evaluation of $\psi_n^{(1)}$s in Eqn. 3.16 requires a knowledge of the full spectrum of Kohn-Sham Hamiltonian and an extensive summation over unoccupied (conduction) bands.

CHAPTER 4

COPPER INTERCALATION INTO HBN

4.1 Statement Of The Problem

The effect of hot pressing of hexagonal boron nitride in a metallic copper environment has been studied with the aim of obtaining Cu intercalated hBN. The results of these experiments are not easy to understand whether an intercalation process takes place or not. Hubacek, Sato and Ueki report a positive effect of Copper on hBN crystallization, and a c-axis preferable alignment which is perpendicular to the uniaxial pressure direction[16]. While Hubacek and Ueki report that the character of the orientation of hBN grains is important for the effect the copper environment, i.e. the effect of copper is macroscopic not microscopic[17]. In another study M-hBN (M: Cr, Mn, Fe, Co, Ni, Cu, Zn, and Ag) compounds were synthesized and crystallinity, grain size, and interlaying spacing of hBN was examined [18]. They reported that transition metal nitrates increased the crystallinity of hBN and arranged the layers of hBN at low temperature (1050°C). On the other hand, Dai et. al. reported the molecular orbital studies of Cu intercalation into hBN by using molecular cluster model and their vibrational analysis indicates that Cu intercalation into hBN is not possible as a stable structure but metastable[19].

In this chapter, we will report a density functional study of copper intercalation into hBN. First, we will give the calculation details and result of the geometry optimization studies then follow by the stability of the system based on the calculated phonon frequencies.

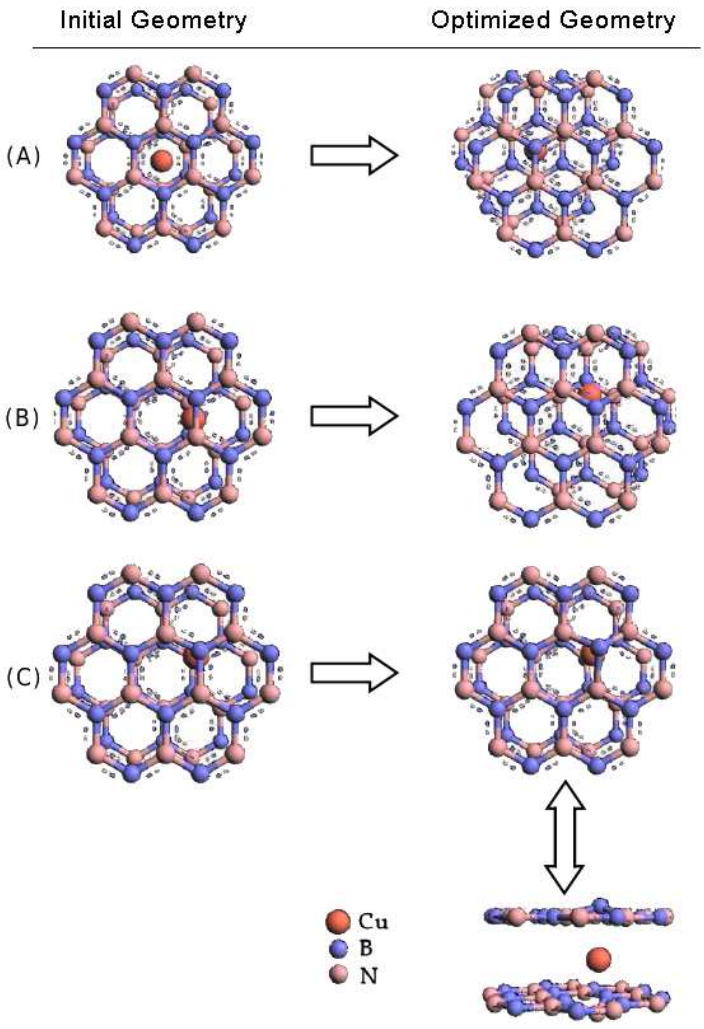

Figure 4.1: Three possible positions for Cu between hBN layers and their optimized geometries.

4.2 Calculational Details

We have considered a unit cell which consist of (32+32) (Boron+Nitrogen) atoms and one copper atom. The system has the periodic boundary conditions, so we are actually calculating Cu-hBN system that has 1.56% Cu intercalation into hBN. The effect of the ions on electrons is accounted by using Troullier-Martins type norm-conserving pseudopotentials, electron-electron exchange-correlation interactions are takes into accounted in local density approximation level. The kinetic

energy cut-off for the plane waves that are used to describe the electronic wave functions is 30 Hartree which was found to be converged at 67 mHa level for the total energy. The Brillouin zone integrations were performed by using [4 4 4] Monkhorst-Pack grid.

At the start, we have taken the equilibrium positions of a cell of 64 atom hBN and considered three different starting positions for the copper atom.

A. Cu atom positioned at the center of the hBN hexagons of each layer as shown in Figure 4.1 (A).

B. Cu atom positioned between the bonds along B and N of each layer as shown in Figure 4.1 (B).

C. Cu atom positioned between the B of the first layer and N of the second layer as shown in Figure 4.1 (C).

The position of the copper, boron and nitrogen atoms were optimized according to the force on them until this force is less than 10^{-4} Ha/bohr. The unit cell dimensions were also adjusted according to BHFGS algorithm to minimize the total energy.

At the optimized configurations, the total energy of the systems are found to be -481.30 Ha, -481.33 Ha, -481.86 Ha in A, B, C configurations respectively. Based on these results, the configuration C is found to be the most stable structure for Cu intercalation into hBN. In this configuration Cu atom is located between a boron atom of one layer and the nitrogen atom of the next layer. Cu-N distance is 4.42 au while Cu-B distance is 4.19 au. This finding is interesting because in all intercalation compounds, the intercalant is located at the void space which is under the hexagons of the honeycomb 2-D lattice of two layers.

The incorporation of Cu seem to affect the B-N bond length and the corrugation of BN layers. d_{BN} for the immediate neighbours of Cu increases from its

bulk value of 2.72 au to 2.92 au. The BN layers above(below) Cu atoms move up(down) by 1.35 au.

Normally one would expect an energy cost for this corruption so that hexagonal locations would be favorable for intercalants, but apparently Cu-B and C-N bond formations reduces the total energy more than corruption increases it.

The contour plots of charge density of the Cu-intercalated hBN is plotted in figure 4.2. here, we plot the 2-D charge density for x-y, x-z, y-z projections as well as a 3-D plot of x-z projection.

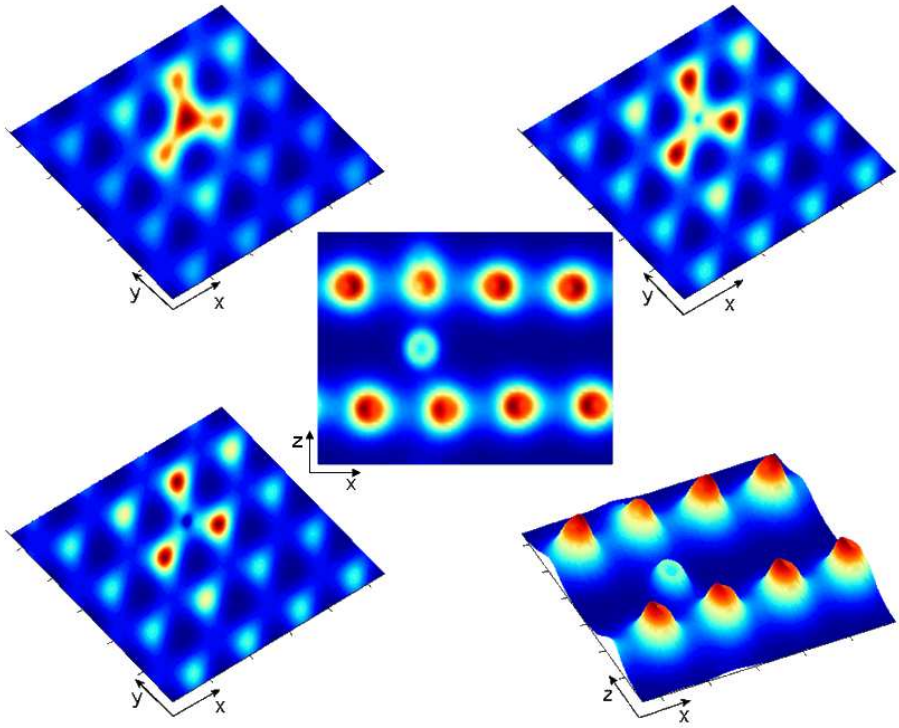

Figure 4.2: Charge densities of the optimized Cu-hBN geometry.

Charge density plots of Figure 4.2 indicates that there are actual bonds formed between the copper and B an N atoms which is again contrary to the usual intercalation mechanism which does not involve any bond formation between the intercalant an the host atoms.

4.3 Stability Of The System

4.3.1 Lattice Dynamical Properties

The stability of a lattice structure can be analyzed by looking up the vibrational frequencies of the normal modes of the atoms that form the crystal. In general, an imaginary atomic vibration frequency indicates a structural unstability because of the for of timedependence of the modes as $\alpha\ e^{-iwt}$. To assess the stability of Cu-intercalated hBN, we have calculated the phonon frequencies of the system that was optimized and discussed in Section 4.2, by using density functional perturbation(linear response) theory which was reviewed in Chapter 3.

Since there are large number of atoms(65 atoms) in the primitive cell that we use, a full calculation of phonon dispersions for the whole Brillouin zone is very demanding and it is not possible with our computational resources. Since our objective is to check the existence of negative frequencies, a calculation done at the zone center might give us idea about the stability of the system. so we have done a single Γ-point lattice dynamical calculation. the results we obtained can be directly compared to the optical vibrational spectroscopic techniques that can measure only zone-center phonons, anyway. The linear response calculations are done by using same set o pseudopotentials as the optimization, at optimized geometry. Since the primitive unit cell contains 65 atoms, there are 65x3=195 normal modes of the system. The calculated frequency of these modes are displayed in Table 4.1. The copper related frequencies can be obtained by comparing the spectrum of pure hBN phonon frequencies at Γ. To make the comparison meaningful, one needs to obtain the zone center frequencies of an hBN unit cell that is 4x4x1 times the primitive unit cell. The Γ phonons of such a structure can be calculated ab initio or by using folding concept. One such study is [20] and we

use their results(Figure 4.3).

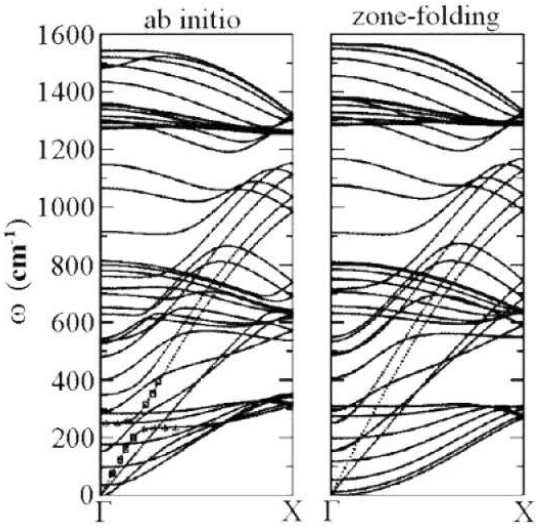

Figure 4.3: Ab inito and zone folding phonon frequencies of hBN.

Based on the data in Figure 4.3 and Table 4.1 the phonons at 187, 560, 960 and 1206 cm^{-1} are Cu-related vibrational frequencies. These can be probed by using Infrared or Raman spectroscopic techniques.

The imaginary frequency modes at 63i indicate that copper intercalated hBN is metastable with respect to the displacements of this particular mode. but one needs to note that the very low frequency of this mode makes it difficult to figure out whether the real system unstable or the DFT-LDA schema is not able to describe the dynamics well because of acoustic sum rule not being satisfied exactly.

To address these questions, one needs to calculate the whole Brillouin zone phonon dispersion relations and make a through convergence study of the phonon bands which is not possible with computing resources at our disposal at the moment.

Table 4.1: Phonon frequencies of Cu intercalated hBN at the Γ point of the Brillouin zone(cm^{-1})

63i	63i	0	0	0
89	89	127	137	138
138	161	163	163	184
187	187	199	199	244
253	268	268	280	283
283	287	287	291	295
296	296	301	301	305
328	328	337	390	390
398	398	399	402	403
403	408	410	426	426
468	468	473	541	541
541	547	560	560	614
615	615	618	618	619
619	626	626	634	646
646	649	651	651	653
662	679	679	693	694
694	702	702	703	703
704	705	711	715	715
717	717	717	724	724
733	733	738	740	740
740	744	746	746	747
761	763	763	769	769
771	804	829	912	912
929	960	960	961	969
970	970	977	980	980
1073	1073	1081	1081	1131
1150	1151	1151	1164	1165
1206	1240	1253	1253	1254
1254	1262	1264	1264	1264
1265	1271	1271	1279	1279
1284	1284	1285	1285	1285
1288	1288	1291	1293	1293
1295	1296	1299	1299	1300
1301	1301	1303	1306	1306
1311	1311	1311	1322	1324
1324	1327	1329	1329	1355
1355	1361	1361	1412	1418
1418	1440	1440	1446	1491
1491	1508	1521	1521	1527

CHAPTER 5

ALKALI INTERCALATION OF GRAPHITE AND HBN - ELECTRONIC PROPERTIES

5.1 Introduction

Graphite intercalation refers to the process of forming a new compound without loss of planarity for the graphene layers, with heteroatoms or molecules residing between the original graphite layers. [21] Hundreds of graphite intercalation compounds (GIC) with interesting structural, electrical and optical properties, have been synthesized and characterized by several experimental and theoretical tools. [22] Alkali and alkaline earth metal-graphite intercalation compounds (AGIC) are formed by charge transfer from the intercalant metal atom to the graphene layers and are among the most widely studied GICs. Among the AGICs, lithium-GIC has technological relevance because of its usage as the anode of rechargeable Li-ion batteries [23]. Discovery of relatively high superconducting critical temperature ($T_C = 11.5$ K) for Ca intercalated graphite [24] has reinvigorated the research in GICs in recent years [25].

The hexagonal form of boron nitride (hBN) is isoelectronic to graphite and their lattice structure are quite similar (graphite: $a = 2.464$, $c = 6.708$; hBN: $a = 2.504$, $c = 6.660$ Å). Because of the partial ionic character of the B and N atoms that form the honeycomb 2-D lattice, interlayer interaction in hBN is stronger compared to that in graphite which is reflected in smaller c_{hBN} compared to c of graphite. Both graphite and hBN layers are found to form nanotube, fullerene and similar structures. [26] Based on similarities between graphite and

hBN there has been quite a number of attempts to intercalate hBN with alkali metals as well as other intercalants without any successfull reports[27, 28]. Based on its lower atomic radius lithium can be considered as the best candidate among all the alkali metals to be intercalated into hBN successfully.

The aim of the present work is to make a detailed first principles investigation of intercalation of metals into hexagonal boron nitride.

The alkali intercalation of graphite has a conceptually simple picture: since layers of graphite are held together with weak van der Walls interaction, the s electrons of the intercalants are transferred to the graphene layers. There has been a number of contraversial issues concerning the electronic structure of the AGICs; namely the amount of the charge transferred from the intercalant to the graphene layer and the role of the interlayer state in the superconducting state. One of the important topics of discussion related to the GICs and Li-GICs in particular is the nature of charge transfer between the intercalated atom and the carbon sheets of graphite. Some experimental [29] and theoretical [30, 31] studies suggest that there is a full transfer of metal s electron to the graphite anti-bonding $\pi^\star$ orbitals, while others conclude that the transfer negligible or only partial [32, 33, 34]. Hightower *et.al.*[32] used electron energy loss spectroscopy to investigate the charge transfer in C_6Li and found that there is no or very little charge transfer from Li to graphite while another experimental study by Ritsko[29] shows full charge transfer for potassium and lithium intercalated graphite systems. Rakotomahevitra *et. al.* [35] calculated the charge transfer by using the extra-orbital model and found the charge transferred from lithium to its neighboring graphite carbons to be $0.454e^-$. Hartwigsen[36] reported that the most of the first stage alkali-GICs have the geometrical charge transfer of around $0.4e^-$ but the physical charge transfer for lithium intercalated graphite was found

to be $0.07e^-$ while the transfer for the other alkalis was found to be $0.2e^-$.

5.2 Computational Setup

All the calculations reported in this thesis were obtained by using ABINIT package[37] which is implementation of density functional theory(DFT) and uses plane-wave basis for the representation of electronic wave functions. The Rappe type optimized pseudopotentials, for describing interaction between electrons and nuclei, were generated by Opium[38] software. Used pseudopotential parameters are given in Table 5.1 for C, B,N and Li atoms. The exchange correlation

Table 5.1: Used number of valance electrons(z_{ion}), cut-off radius (r_{cut}) of orbitals and occupation of electrons in each orbital(# e^-) for pseudopotential generation)

Atom	z_{ion}	r_{cut} (1s)	r_{cut} (2s)	r_{cut} (2p)	# e^- (1s)	# e^- (2s)	# e^- (2p)
C	4.00	-	1.45	1.55	-	2.00	2.00
B	3.00	-	1.14	1.49	-	2.00	1.00
N	5.00	-	1.35	1.54	-	2.00	3.00
Li	3.00	1.45	1.45	1.45	2.00	1.00	-

energy is evaluated in local density approximation(LDA), using Perdew-Wang parametrization[39] of Ceperley-Alder electron-gas data[40]. The number of k-points for graphite,C_6Li and C_3Li are 42, 15, 150 and cutoff energies are 45 Ha, 40 Ha and 50 Ha respectively. Number of k-points for the hBN and corresponding Li-intercalation compounds $(BN)_3Li$ and $(BN)_6Li_4$ are 42, 120, 195 and cutoff energies are 45Ha, 40Ha and 40Ha respectively. All the parameters are obtained after k-point and cutoff energy convergence studies which is enough for the convergence of total energy (10^{-3} Ha).

For all the compounds of Li intercalated graphite and hBN, we have done convergence calculations which refer as to call reciprocal space sampling. Reciprocal space sampling is depends on the geometry. For these purpose, minimum energy was calculated for the different number of k-points at cutoff energy 45 Hartree.

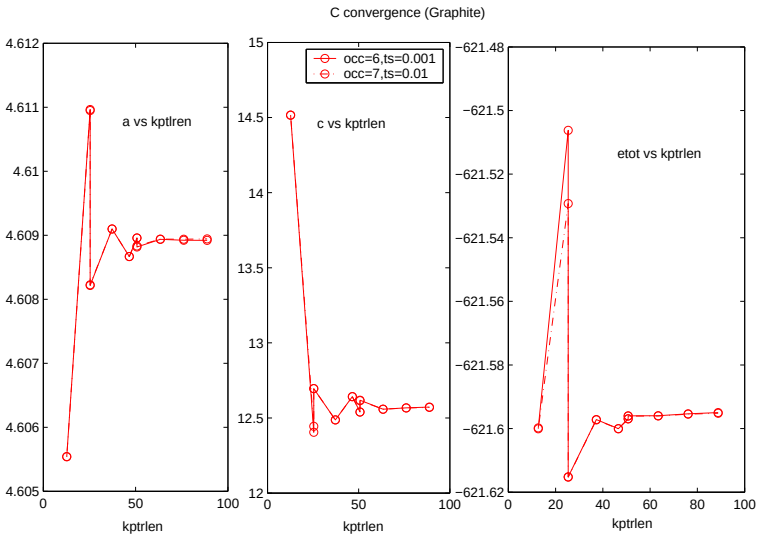

Figure 5.1: Convergence plot of carbon in graphite form.

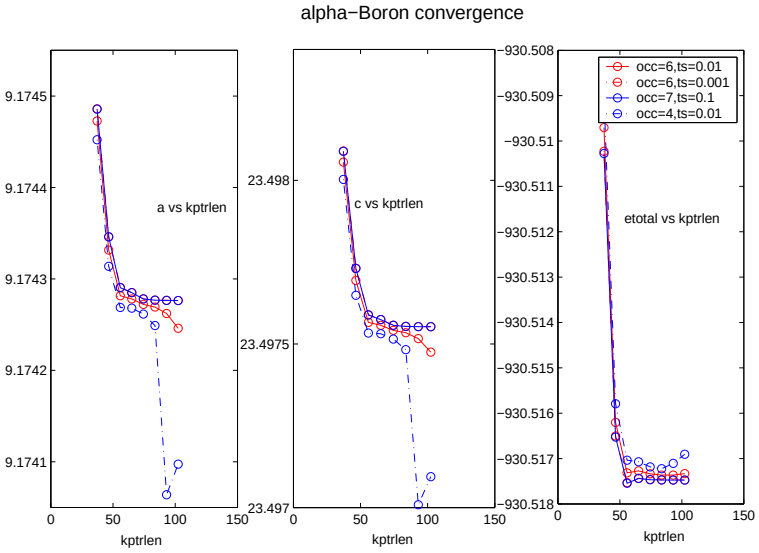

Figure 5.2: Convergence plot of α-Boron.

Energy and convergence as quality of k-point mesh for each smearing factor and occupation option are given in Figures 5.1$\sim$ 5.9.

As can bee seen from all the convergence plots, cell parameters were converged from a kptrlen value of 50 to 80 which gives the number of k-points as 28, 36, 26, 30, 19 for α-boron, N_2, bcc-Lithium, hcp-Lithium and fcc-Lithium respectively.

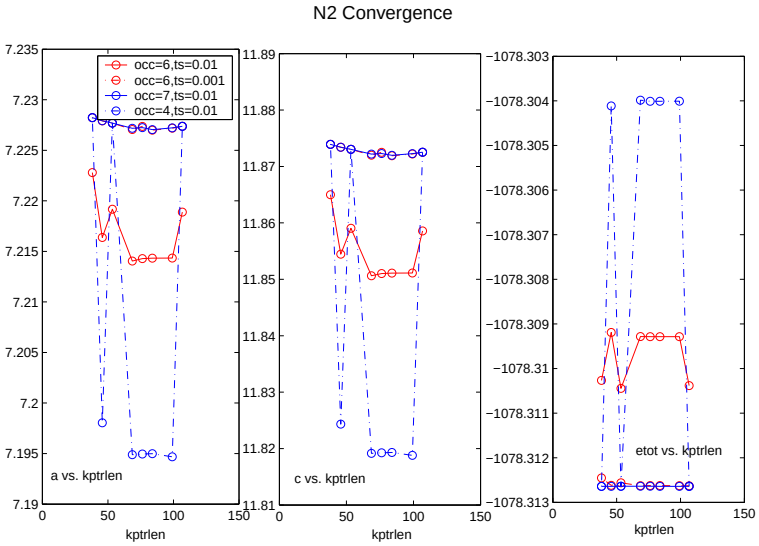

Figure 5.3: Convergence plot of Nitrogen dimer(N_2).

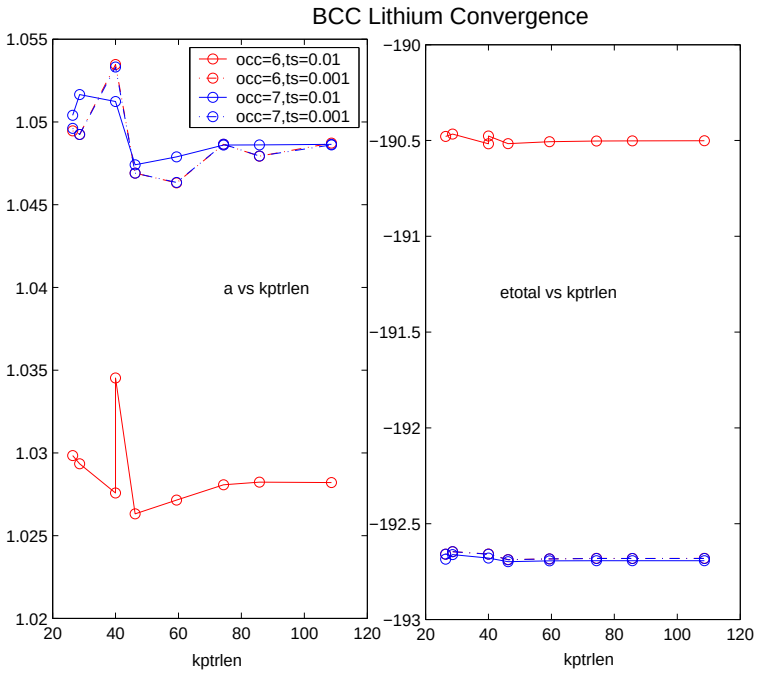

Figure 5.4: Convergence plot of lithium in bcc structure.

The kptrlen parameter is the parameter which characterize the reciprocal space sampling with smallest distance of k-points in real space. The larger k-point is the finer is the grid in reciprocal space. For energy convergence we need more

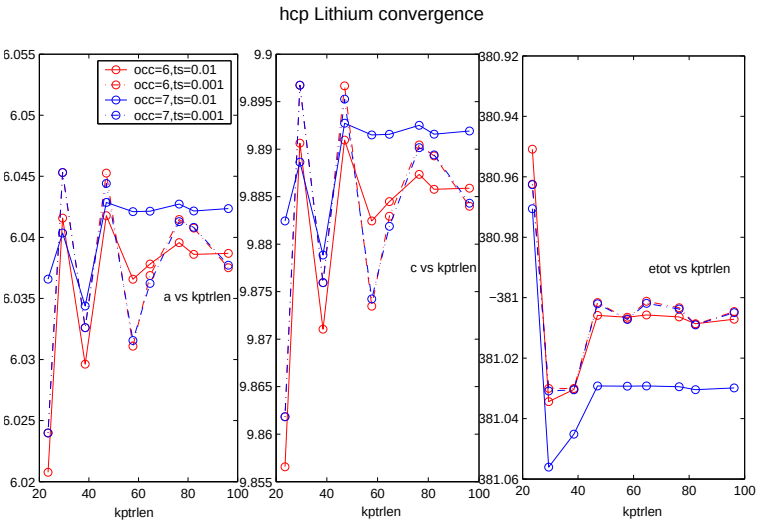

Figure 5.5: Convergence plot of lithium in hcp structure.

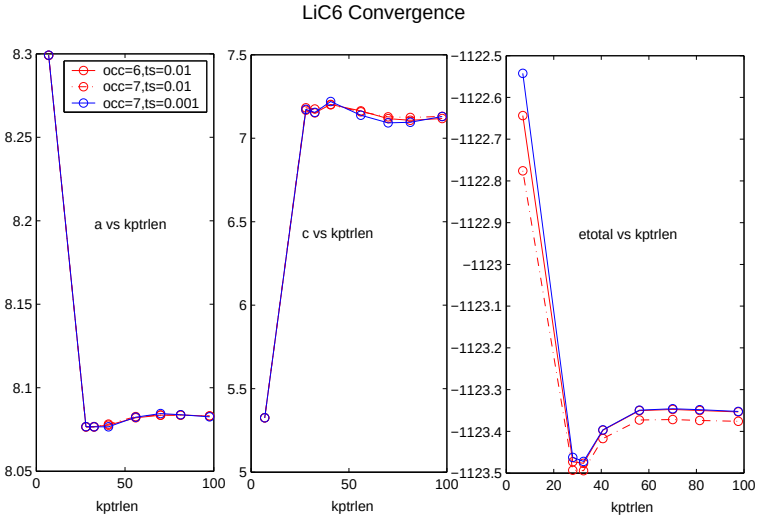

Figure 5.6: Convergence plot of C_6Li.

sensitive convergence criteria because of the binding energy on the order of couple of tens of meV. For the solid phases of C an Li, the convergence was reached at kptrlen=50 and corresponding graphite and hBN intercalation compounds reached the convergence number of k-points 42, 15, 30 for graphite, C_6Li and C_3Li and 28, 40, 36 for hBN, $(BN)_3Li$ and $(BN)_6Li_4$ respectively. The difference of total energies after this number of k-point is below 0.1 meV which is acceptable

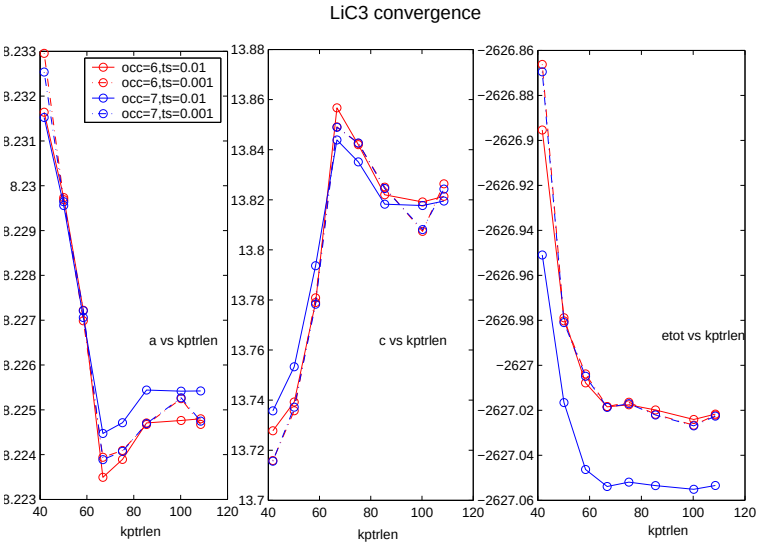

Figure 5.7: Convergence plot of C_3Li.

according to binding energy criteria.

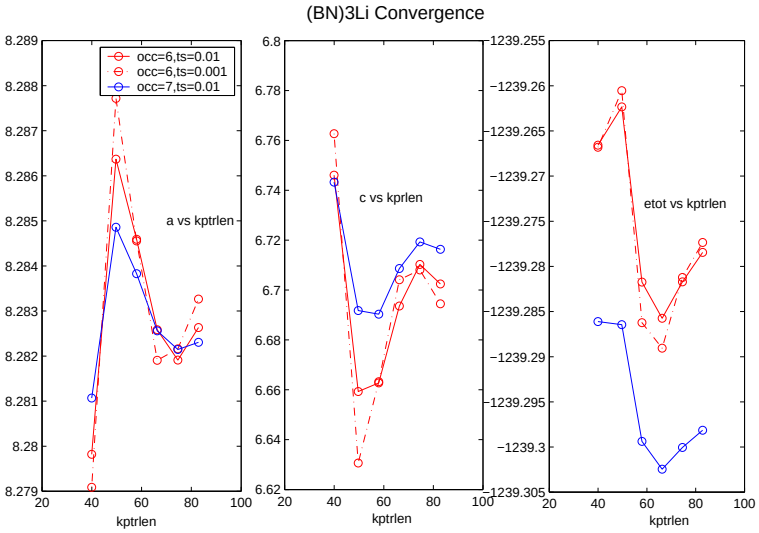

Figure 5.8: Convergence plot of $(BN)_3Li$.

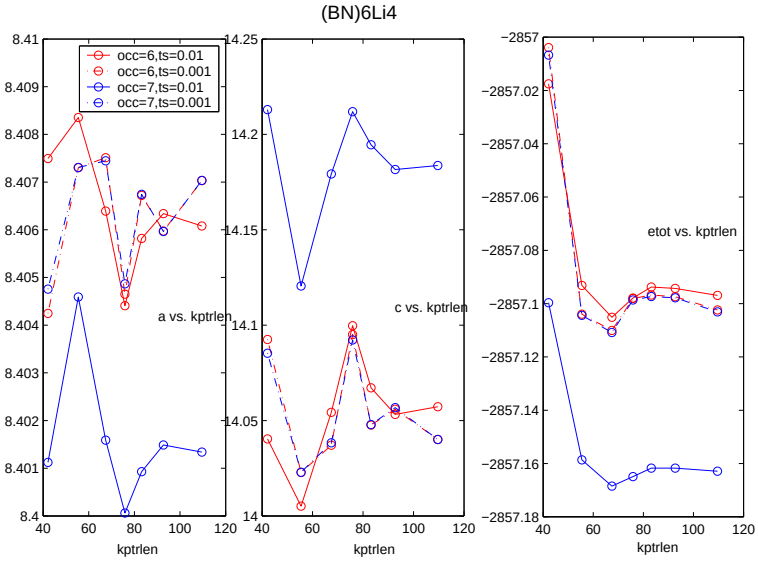

Figure 5.9: Convergence plot of $(BN)_6Li_4$.

5.3 Results

5.3.1 Lattice geometry

The crystal structure information on the compounds studied in the present work are given in Table 5.2 for graphite, C_6Li and C_3Li and Table 5.3 for hBN, $(BN)_6Li_4$ and $(BN)_3Li$. The space group and Wyckoff position information for C_6Li and C_3Li are taken from literature [41, 42]. The hypothetical Li intercalated compounds of hBN are formed by simply replacing the proper C atoms with equal number of B and N atoms. Then the lattice parameters are relaxed according to BFGS algorithm [43, 44, 45, 46] to minimize the total energy of the cell. The obtained a and c values are given in Table 5.2 and Table 5.3. The relative error of the results range from 0.47% for (a of hBN) to 2.86% for (c of C_6Li), which are in the limits of DFT calculations. A well-known weakness of DFT is related to the absence of dispersion forces which are important for layer-layer interactions in graphite. As expected LDA overestimates c, i.e. under-binds the layers. We have done some calculations with a GGA exchange correlation potential, the re-

sults, which are not reported here similar, but lattice dynamical properties were produced very poorly with GGA, so we only report LDA results.

It should be noted from the Table 5.2 and Table 5.3 that the order of lattice parameters between the graphite and hBN (a_{hBN} is greater than $a_{graphite}$ and c_{hBN} less than $c_{graphite}$) is also observed for their intercalation compounds' parameters except for the C_3Li analogue of $(BN)_6Li_4$ which has $c_{(BN)6Li4}$ is greater than c_{C3Li}.

Table 5.2: Lattice parameters of graphite, C_6Li and C_3Li

	Graphite	C_6Li	C_3Li
Symmetry	$P6_3/mmc$	P6/mmm	P-62m
Wyckoff positions	C_1:2c C_2:2d	Li:1b C:6k	Li:4f C:6j
This work a(au)	2.439	4.275	4.422
This work c(au)	6.653	3.812	7.494
Exp. a(au)	2.460[a] 2.463[d]	4.305[b]	4.30[g]
Exp. c(au)	6.700[a] 6.717[d]	3.706[b]	7.40[g]
Theo. a(au)	2.470[e] 2.447[f]	4.300[c] 4.300[c*]	4.41[g]
Theo. c(au)	6.600[e] 6.660[f]	3.700[c] 3.800[c*]	7.488[g]

[a]Ref.[47], [b]Ref.[48], [c]Ref.[49]xc:LDA, [c*]Ref.[49]xc:GGA-PW, [d]Ref.[50], [e]Ref.[51], [f]Ref.[52], [g]Ref.[53]

5.3.2 Formation energy and enthalpy

Cohesive energy of a compound is defined as the energy gain, per atom, of creating the compound in the given lattice structure from the isolated spin-polarized atoms that constitute the compound:

$$E_c = E_t - E_x - E_y$$

Table 5.3: Lattice parameters of hBN, $(BN)_6Li_4$ and $(BN)_3Li$.

	hBN	$(BN)_3Li$	$(BN)_6Li_4$
Symmetry	$P6_3/mmc$	P-62m	$P6_3/m$
Wyckoff positions	B:2c N:2d		
This work a(au)	2.493	4.384	4.487
This work c(au)	6.509	3.541	7.797
Exp. a(au)	2.506[a] 2.505[b]		
Exp. c(au)	6.692[a] 6.660[b]		
Theo. a(au)	2.490[c] 2.504[d] 2.478[e]		
Theo. c(au)	6.420[c] 6.660[d] 6.568[e]		

[a]Ref.[54], [b]Ref.[55], [c]Ref.[56], [d]Ref.[57], [e]Ref.[58]

where E_x is the total energy of the atom x and binding enthalpy(formation energy) of a compound

$$\Delta H = E_t - E_x^{solid} - E_y^{solid}$$

where E_x^s is the total energy of the atom x in the solid phase.

The single atom total energies for Li, B, C are calculated in spin-polarized state by placing the atom in a cubic box of lattice constant 15 Å. For nitrogen, we have used a nitrogen dimer in the cubic box as the atomic limit. We have used a single $k-$ point (Γ) for all the Brillouin zone integrations in the atomic total energy calculations.

The formation enthalpy and the cohesive energies for graphite, hBN, C_6Li, C_3Li, $(BN)_6Li_4$ and $(BN)_3Li$ calculated from the atomic energies of the elements and the solids of these elements as detailed above are given in Table 5.4. Experimental data on the enthalpy exist only for C_6Li and is -13.9 kj/mol[41]. One

important finding of enthalpy results is that both hBN intercalation compounds have positive formation energy which indicates that for these compounds to form one needs to provide energy externally. The positive formation energy is the probably cause of the difficulty of intercalating hBN which might be overcomed by applying high pressure.

Table 5.4: Cohesive energies and formation energies of graphite, hBN, C_6Li, C_3Li, $(BN)_6Li_4$ and $(BN)_3Li$.Formation energies,$E_f^\star$, calculated from graphite and hBN total energies instead of the energy of atoms(B,N and C) itselves.

	Graphite	hBN	C_6Li	C_3Li	$(BN)_3Li$	$(BN)_6Li_4$
E_c (eV)	-8.41	-8.56	-7.21	-6.17	-7.14	-6.02
E_f (eV)	-	-1.368	-0.082	-0.014	-1.06	-0.774
$E_f^\star$ (eV)	-	-1.368	-0.082	-0.014	0.112	0.253

The binding energy of the compounds considered in this study are around 0.1 eV, one needs very high convergence in the total energies. To reach this convergence level at the total energy, i have done the energy calculations for solid phase Li, B and N for the different number of k-points and obtained the most acceptable converged energy.

The total energy of solid phase lithium in bcc, fcc, hcp structures are determined and results are given in Table 5.5 with its lattice parameters. The lowest energy configuration is found to be the hcp phase with a difference $E_{\rm fcc} - E_{\rm hcp} =$ 13 meV and $E_{\rm bcc} - E_{\rm fcc} = 12$ meV. The same set of calculations were done by using GGA exchange-correlation as well as LDA HGH pseudopotentials and the same ordering with similar energy differences were found.

Elemental boron in its solid form has many crystallographic polymorphs which has been the subject of many recent studies [64, 65, 66]. Although there is no consensus on the low temperature structure, we have considered α-boron structure as the ground state phase of boron similar to Refs. [64, 65]. α-boron has a rhombohedral Bravais lattice with the space group $R\bar{3}m$ (no. 166). The basis

Table 5.5: Structural parameters of bulk lithium. The lowest energy structure is indicated with the star superscript.

	Structure	a_0 (au)	B(kbar)	B'	E_C(eV)
This work	hcp*	6.03 (c/a=1.637)	120.95	3.21	1.635
	fcc	8.54	117.7	3.50	1.622
	bcc	6.78	122.95	3.49	1.610
Experimental	hcp[a]	5.88 ($c/a = 1.637$)	126.5		1.687
	bcc	6.60[b]	116[b]		1.659[c]
Theory[d]	hcp	5.64 ($c/a = 1.633$)	149.7		1.860
	fcc	8.03	148.2		1.851
	bcc	6.35	148.2		1.837

[a]Ref.[59],[b]Ref.[60],[c]Ref.[61] is referred in [62],[d]Ref.[63]

of the crystal is a icosohedral B_{12} boron unit. The optimized structural parameters along with experimental data and the results of other DFT studies are given in Table 5.6. The agreement between the experiment and the DFT results is excellent.

Table 5.6: Structural parameters of bulk boron.

	a_0 (au)	α (degrees)	B(kbar)	B'	E_C(eV)
This work	9.45	58.15	240.0	2.29	6.54
Theory[a]	9.39	58.06	218.4	4.8	6.95
Exp.[b]	9.56	58.65	213-224	4.00	5.81
Exp.[c]	9.56	58.06			

[a]Ref.[64],[b]Ref.[48],[c]Ref.[67]

The reference energies for nitrogen are calculated for N_2 dimer phase in a cubic box of side 15 Å for the gas phase and a hexagonal closed pack structure with dimers aligned along the z-direction for the condensate phase and display the results along with experimental and previous theoretical results in Table 5.7.

Table 5.7: Bond length, vibrational frequency and cohesive energy of nitrogen dimer.

	d (au)	ω(THz)	E_C(eV)
This work	2.06		-8.27
Theory[a]	2.10	464.3	-11.33
Exp.[b]	2.08	444.8	-9.9

[a]Ref.[68],[b]Ref.[69]

5.3.3 Charge Transfer

Although there is no quantum mechanical observable associated with the charge density of an individual atom in a compound, various heuristic methods have been devised and used as an essential tool for understanding many of the properties of materials. Electronic orbital based Mulliken [70] and Lowdin [71] charges as well as electronic charge based Hirshfeld [72] and Bader [73] charges are most widely used charge partitioning schemes. Hartwigsen *et. al.* [36] used DFT-LDA to investigate the charge transfer in AGICs with the help of Bader's atom-in molecule construction to define the atomic volumes and found that 0.5 e is transferred from Li to the graphene and the transfer is mostly due to geometrical consequences. Sun *et. al.* [30] have calculated the charge transfer to be complete by comparing the integrated density of π states for the pristine and Li-intercalated graphite in a DFT-GGA calculation. Chan *et. al.* have used first principles calculations and diffraction experiments to show that the charge transfer in alkali graphite intercalation compounds can be related to the change in C-C bond length in AGICs compared to that in pristine graphite. [74, 75] Soft X-ray emission spectroscopy [76] Some experimental[29] and theoretical [30, 31] studies are thought to indicate a full charge transfer of the metal *s* electrons to the graphite, while the others show no or negligible charge transfer or partial charge transfer[33, 34, 32].

Early ARPES data [77] indicate that lithium in C_6Li is essentially Li^+ ion which indicates a full charge transfer.

Hightower *et. al.* [32] have investigated the charge transfer in C_6Li by using transmission electron energy-loss spectrometry and found negligible charge transfer from Li to the graphite layers. We have calculated the Hirshfeld[78, 72, 79] charges for intercalated compounds and display the results in Table 5.8. In the Hirshfeld method, total electron density of the system is shared between the dif-

ferent atoms of the system. Simply defined as difference between "charge density of the bonded atom" and the "atomic density", in other words the density difference between the free atom and the bonded atom, and can be used as indication of the transfer of electronic charge between the atoms in forming the solids. In C_3Li and C_6Li, it is found that only 0.184 and 0.225 e^- from Li are transferred to the carbon sheets which gives a 0.031 and 0.076 e^- charge for each of the carbons. The finding is in disagreement with studies that report full charge transfer Refs.[30, 31]. It is known that Hirshfeld charges underestimate the amount of charge transfer by a factor of 2 [80]. Similarly, the Hirshfeld charges of hBN

Table 5.8: Hirshfeld charges of bulk and Li intercalated graphite and hBN systems.

Compound	B	N	Li
hBN(Bulk)	0.28	-0.28	-
$(BN)_3Li$	0.09	-0.16	0.21
$(BN)_6Li_4$	0.04	-0.16	0.17
Compound	C	Li	
Graphite	0.00	-	
C_3Li	-0.06	0.19	
C_6Li	-0.04	0.24	

and its intercalated compounds indicate that charge lost by the lithium atom are 0.226 an 0.179 electrons for $(BN)_3Li$ and $(BN)_6Li_4$, respectively. Comparing the transfer of charge for C_3Li and C_6Li with $(BN)_6Li_4$ and $(BN)_3Li$, the ordering of the magnitudes are similar. One interesting result in hBN is the change in the character of charge transfer from pure hBN to intercalated compounds. While N is found to transfer 0.28 $e^-$to B in hBN, N gains net 0.16 e^- when Li intercalation takes place and B becomes a net exporter of electrons.

Charge transfer can also be studied by looking at the value of the integrated partial density of electronic states at the Fermi energy. For all four intercalation compounds, we have found that lithium atoms loose around 0.7 electrons which

is independent of the system.

5.4 Electronic Structure

The band structure along high symmetry directions of pure graphite and hBN as well as their Li-intercalated compounds and their partial density of electronic states are displayed in Figures 5.11-5.18. The first Brillouin zone of graphite, C_3Li and C_6Li are overlayed and given in figure 5.10 to base the comparison of band structures. As the c of C_6Li approximately in the smallest, the tallest in the Brillouin zone of C_6Li. The 5.10 is helpful in delineating the relation between the special points of the band structures that will be presented below figures 5.11-5.18.

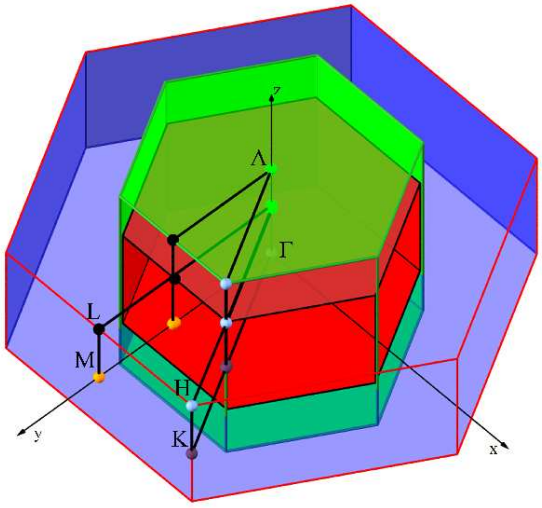

Figure 5.10: First Brillouin zones of graphite(Blue), C_6Li (Green) and C_3Li(Red) with special points.

5.4.1 Graphite and hBN

In this section, we present and compare the electronic structure of the host compounds for the intercalation. The electronic band structure and the angular

momentum resolved density of states for graphite are shown in Fig. 5.11. The electronic structure of graphite has been studied experimentally[81, 82, 83] and theoretically[82, 84, 85, 86] by using many different approximations by several groups over the years. The most important finding of these studies can be summarized as follows: The valence (conduction) bands are formed by $\sigma(\sigma^\star)$ and $\pi(\pi^\star)$ bonding (anti-bonding) orbitals which makes graphite a semi-metal with band overlap of 0.01 eV at the K point of the Brillouin zone. The dispersion of the bands along the c-axis (weak) and in the basal plane (strong) are result of covalent sp^2 bonding in $(x-y)$ plane versus the weak van der Waals interaction between the layers along the $z-$direction. Our calculated band structure for graphite is in good agreement with previous DFT-LDA calculations such as Refs. [82, 87, 88] and reproduces the experimental findings reasonably well.

The electronic band structure of hBN, although subject of many studies, has been controversial[89, 90, 91, 92]. Band gap energies in the range from 3.2 to 5.97 eV have been reported. GW calculations indicate an indirect band-gap semiconductor, while Watanabe *et. al.* [93] have found that hBN is a direct gap semiconductor based on photoluminescence spectroscopy. Our calculated band structure, total and projected density of electronic states for hBN are presented in Fig. 5.12a) and b), respectively. Similar to that of graphite, the band structure of hBN can be interpreted in terms of bonding and anti-bonding σ and π states. The main difference between the two stems from the partial ionic character of B-N bonds which create a band-gap between the bonding and antibonding π states that for the highest (lowest) valence (conduction) bands in hBN. At the LDA level, hBN is found to be an indirect band-gap semiconductor with the minimum gap between the top of the valence band near point K (T_1) and the bottom of the conduction band at point M is found to be 4.06 eV which is in good agreement

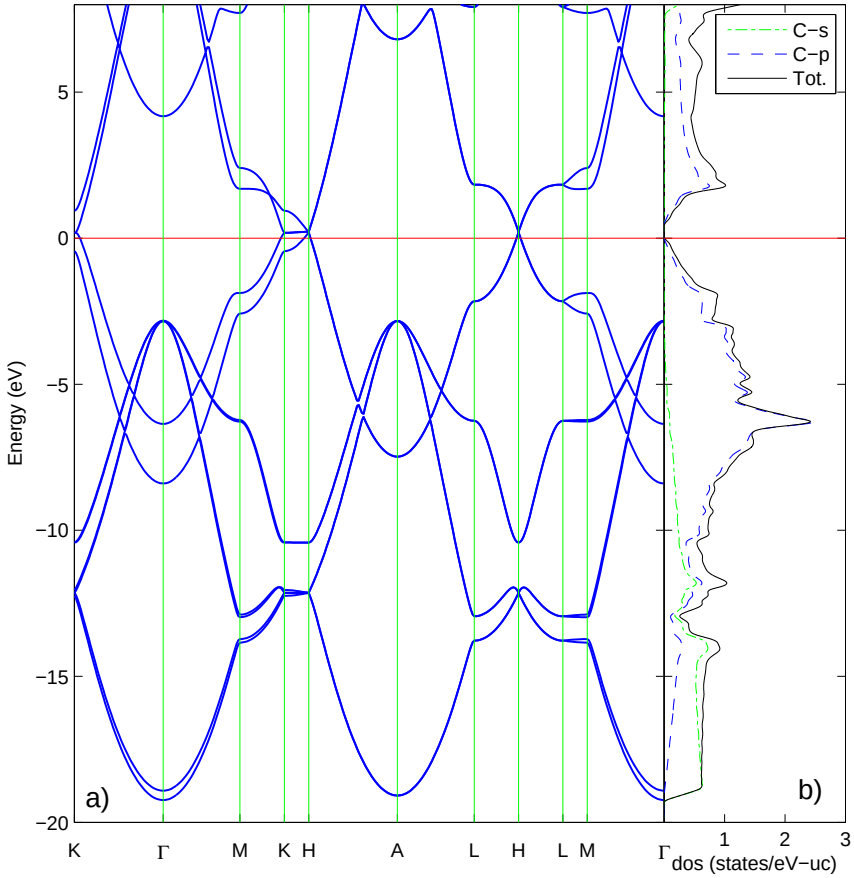

Figure 5.11: Band Structure and pdos of Graphite.

with the previous LDA calculations [89, 90]. The minimum direct band gap is calculated to be 4.50 eV at the M point which is very similar to the direct band gap at H which is 4.53 eV. The direct band gap at the Γ point is 6.48 eV which is close to the GW value reported in Ref. [94]. Sizeable differences in the width of the whole conduction, bottom σ, top σ and π bands can be observed from Fig. 5.11a) and 5.12a). ΔE_{σ_1}, $\Delta E_{\sigma_{2,3}}$ and ΔE_{π} for hBN are found to be 3.10, 2.52 and 2.03 eV narrower than those for graphite. The difference in the bandwidth of the whole conduction band is smaller (19.24 eV for graphite vs 17.70 eV for hBN) compared to the indiviual bands.

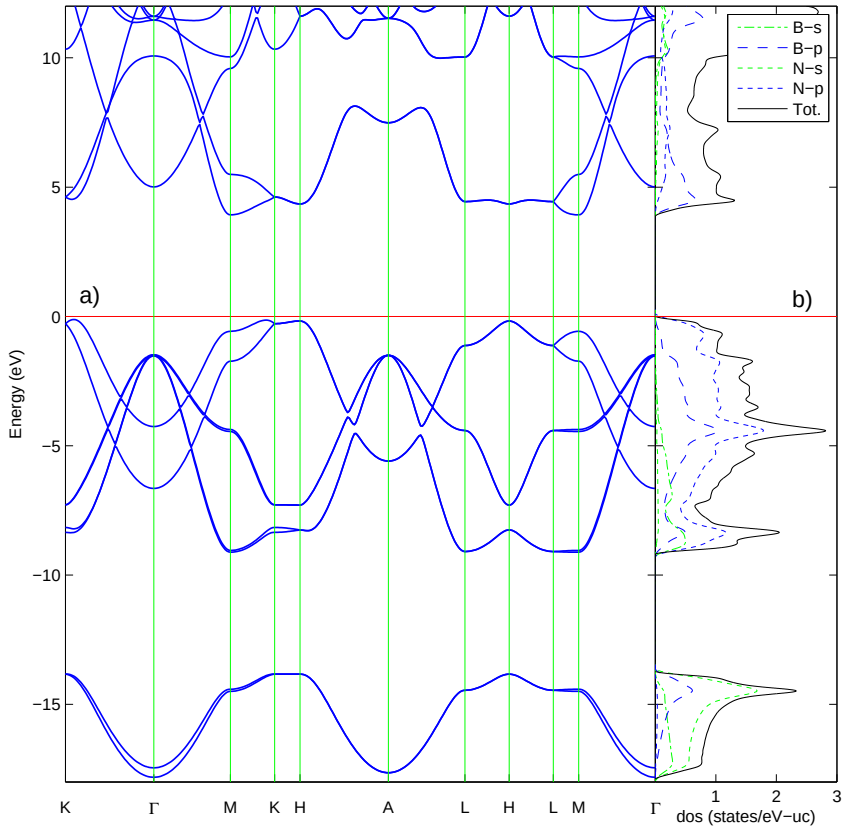

Figure 5.12: Band Structure and pdos of hBN.

The calculated electronic density of states of hBN in Fig. 5.12b) indicates that the top of the valence band is formed mostly from π states localized on nitrogen while the bottom of the conduction bands are formed by $\pi^\star$ states which are mostly on boron atoms.

The lowest conduction band at the center of the Brillouine zone for both graphite and hBN has a nearly free electron like dispersion and named as interlayer state because probability density associated with its wavefunction is mostly located in the midway between the layers that form hBN and graphite. The these wavefunctions are shown in Figures5.13, 5.14 clearly display and interlayer state in both graphite and hBN. Interlayer state was reported to be important in both

intercalation and superconducting properties[95, 96] and will be discussed in the context of lithium intercalation below.

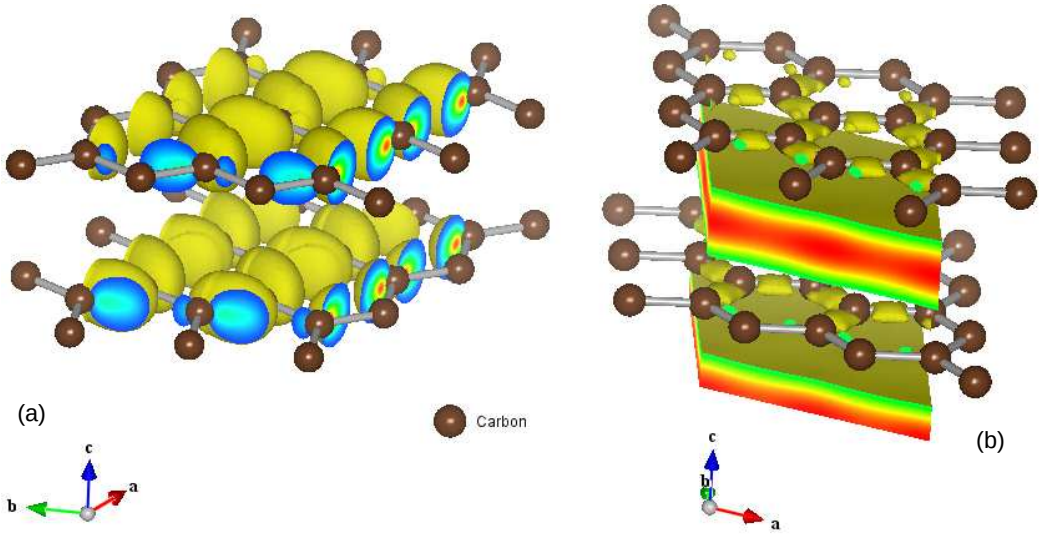

Figure 5.13: Band characters of graphite. (a) Character of state 8 at point K (b)Character of state 9 at point Γ.

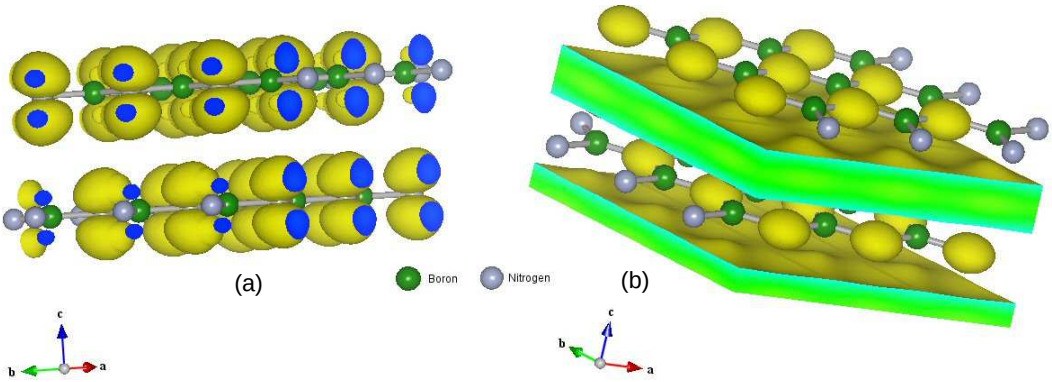

Figure 5.14: Band character of hBN. (a) Character of state 8 at point K (b)Character of state 9 at point Γ.

5.4.2 C_6Li and $(BN)_3Li$

The calculated band structure and partial density of states of C_6Li and C_3Li are displayed in Figures 5.15 and 5.17, respectively. As Holzwarth *et. al.* [97, 98] have

demonstrated nicely, the electronic band structure of alkali intercalated graphite can be deduced from the zone-folding considerations to a great extent. Since the area of the basal plane of C_6Li is three times larger than that of graphite, the volume of the first Brillouin zone of C_6Li is one third of that of graphite and two equivalent K points of graphite BZ are folded back into the zone center. Although the bands of C_6Li are mostly obtained from folding of the graphite bands, there are some notable modifications of the bands around the Fermi level caused by the intercalant lithium. The Fermi energy of C_6Li is raised by approximately 1 eV compared to graphite due to electron donation from lithium. The number of states at the Fermi level is found to be $n(E_F)$=1.31 states/eV. This value is comparable to the results of Pauli susceptibility measurements of Delhaes *et. al* [99]) which is 1.26 states/eV .

Table 5.9: Characteristic energy levels(eV) at Γ point for graphite and C_6Li relative to the Fermi energy.

	Graphite			C_6Li			
Sym.	Exp.	Theo.[a]	T.W	Exp.[b]	Theo.[c]	Theo.[d]	T.W.
$\pi^\star$	0.0	0.0		-0.5	-1.3	-0.9,-1.7	-1.62,-1.16
$\sigma_{2,3}$	-4.6[b],-5.5[a]	-3.04	-3.73	-5.0	-5.9	-5.0	-4.42
π_1	-7.2[a],-5.7[f],-6.6[e]	-6.52	-7.80	-9.3	-9.3	-9.1	-9.05
π_1	-8.1[b],-8.5[e]	-8.58	-9.17				
$\sigma^\star{}_{2,3}$				-13.0	-13.3	-12.6,-11.9	-12.12,-11.85
$\sigma^\star{}_1$						-14.0	-13.62
$\sigma^\star{}_1$,$\sigma^\star{}_{2,3}$				-15.2	-14.9	-14.2	-14.01
$\sigma^\star{}_1$	-20.6[b]	-19.44	-20.12	-22.5	-21.8	-21.1	-20.74

[a]Ref. [100],[b]Ref. [77], [c]Ref. [97, 98],[d]Ref. [101], [e]Ref. [102],[f]Ref. [103], T.W. : This Work

Energy levels of several bonding and anti-bonding π and σ states of C_6Li and graphite are given along with experimental and other theoretical results in Table 5.9. The agreement between our results and the literature is reasonable. For the graphite except the $\sigma_{2,3}$ level there is a good agreement between the calculated and the measured energy levels. While for C_6Li the most pronounced difference between the calculated and measured levels is at $\pi^\star$ state(experimental -0.5 eV while calculated -1.16 eV).

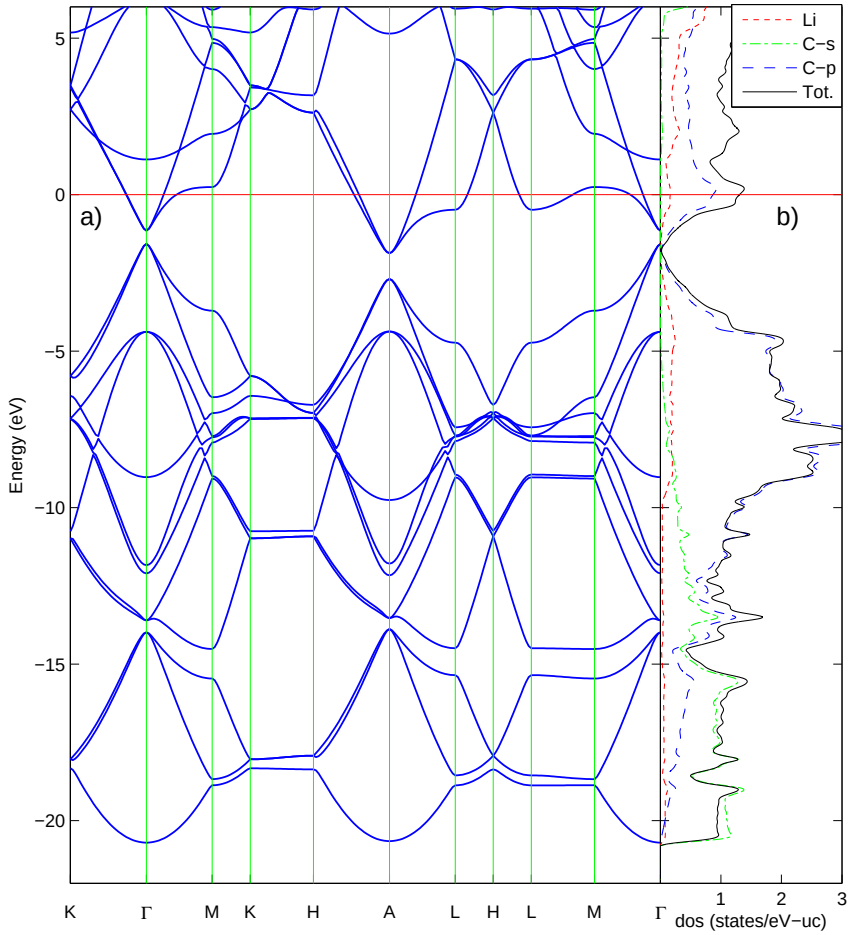

Figure 5.15: Band Structure and pdos of C_6Li.

The dispersion of the bands along the $c-$ and $a-$ axis of the Brillouin zone are quite different. Along K-H, L-M and Γ-A, k_x and k_y are constant and k_z changes from zero to π/c. Non-dispersive nature of conduction bands along these directions indicate the weakness of the interlayer interactions, which is more pronounced for the σ states that are planar on the carbon layers, π and $\pi^\star$ states show a dispersion on the level of 0.75 eV along Γ-A direction for graphite and 1.12 eV for C_6Li.

Higher dispersion in z-direction for C_6Li indicates the effect of Li intercalant

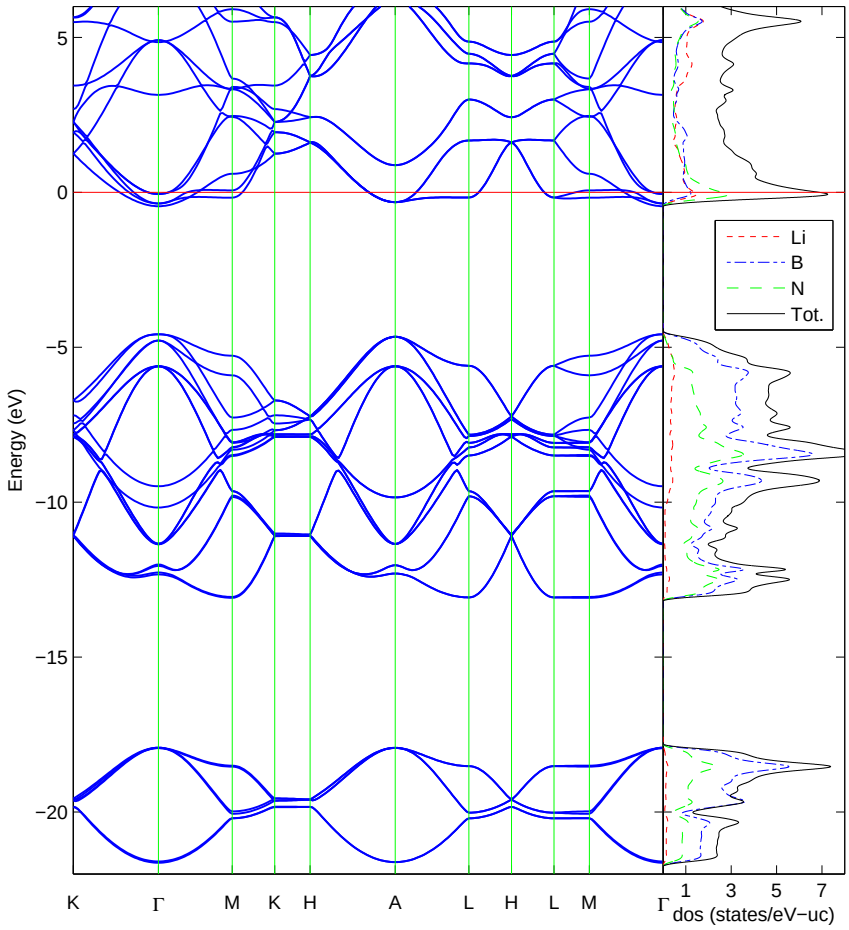

Figure 5.16: Band Structure and pdos of $(BN)_3Li$.

as it intermediates the interaction along this direction. Along K-H, the top of the valance band which is derived from the $\pi^\star$ state has a dispersion of 1.18 eV which is an indication of interaction with the lithium 2s states.

5.4.3 C_3Li and $(BN)_6Li_4$

The calculated band structure of C_3Li is shown in Fig. 5.17. Comparing it with that of C_6Li and graphite reveals a number of differences. Since C_3Li has 16 atoms per primitive unit cell, it has proportionally higher number of valance

bands. The overall structure of the bands of C_3Li is similar to those of C_6Li, especially at energies below -10 eV, the states are predominantly carbon s-derived and intercalation does not change their shape or energy. The states near the top

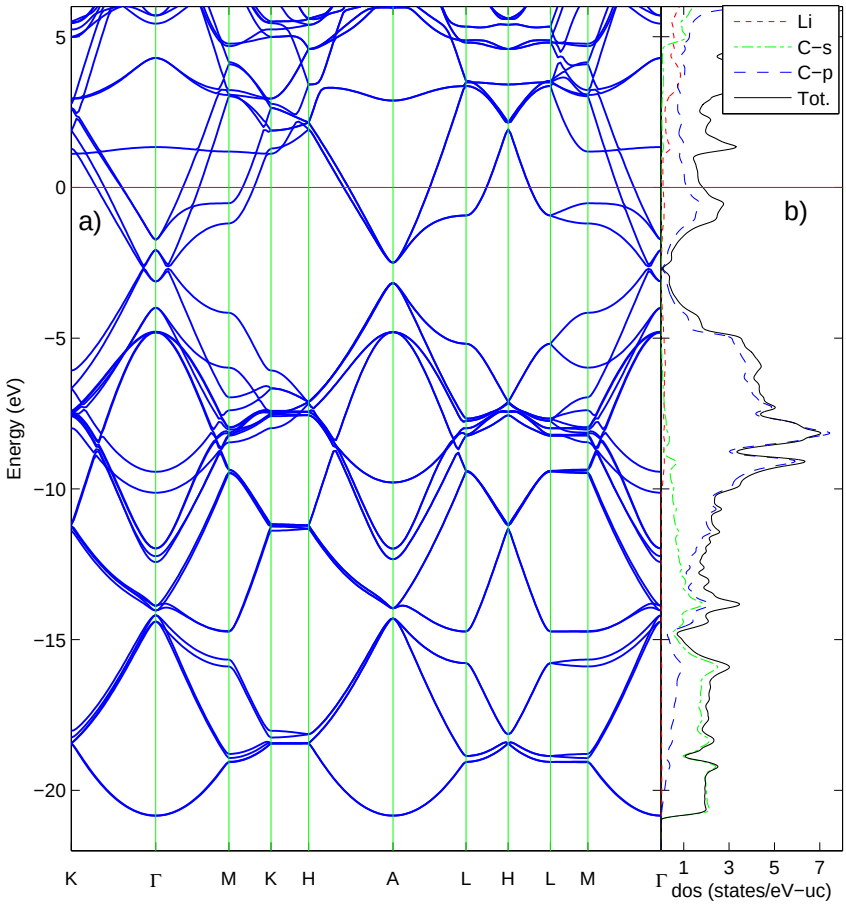

Figure 5.17: Band Structure and pdos of C_3Li.

of the valance band and the bottom of the conduction band show a number of modification compared to C_6Li and graphite; these are, the Fermi energy of C_3Li is raised by 2 eV which is due to the extra electron provided by lithium.

The dispersion of the bands along the Γ-A, L-M and K-H directions for C_3Li show similar trend as in C_6Li. The $n(E_F)$=2.06 states/eV for C_3Li which is higher from that of C_6Li.

The band structure and electronic density of states for hBN analogues of C_6Li and C_3Li ($(BN)_3Li$ and $(BN)_6Li_4$,respectively) are shown in Figures 5.16 and 5.18. The most important difference between the properties of $(BN)_3Li$ and $(BN)_6Li_4$ compared to the hBN(Fig.5.12) is the metallic character of these intercalation compounds as revealed by Fermi level structures in Figures5.16 and 5.18. The number of states at the Fermi level is found to be $n(E_F)$=1.10 for $(BN)_3Li$ and 4.08 states/eV for $(BN)_6Li_4$. These values are somewhat higher than the corresponding GICs. Comparing the valance states near the Fermi level for C_6Li(Fig.5.15) and $(BN)_3Li$ (Fig.5.16), they show a similar structure along the H-A-L directions. The most important difference between the two is π derived states are occupied at Γ for C_6Li while they are empty for $(BN)_3Li$.

The energy levels of $\pi^\star$, $\sigma_{2,3}$, π_1,$\sigma^\star{}_{2,3}$ and $\sigma^\star{}_1$ are different for $(BN)_3Li$ compared to C_6Li because of the insulating character of the host compound (hBN).

Overall the electronic structure of $(BN)_3Li$ can be obtained by folding the band structure of hBN(Fig. 5.12). Lithium intercalation modifies the states near and above the Fermi level as also indicated by the local density of states displayed in Fig. 5.16 for lithium.

The dispersion of the bands along the z-direction for hBN intercalation are found to be similar in character and magnitude to those in GICs. The states that show highest dispersion along Γ-A, L-M and K-H directions are 1.38 eV,1.27 eV and 1.67 eV which are comparable to those of GICs (1.12 eV, 1.99 eV and 1.18 eV). The interaction along z-direction for hBN seems to be stronger than that in graphite except along L-M direction.

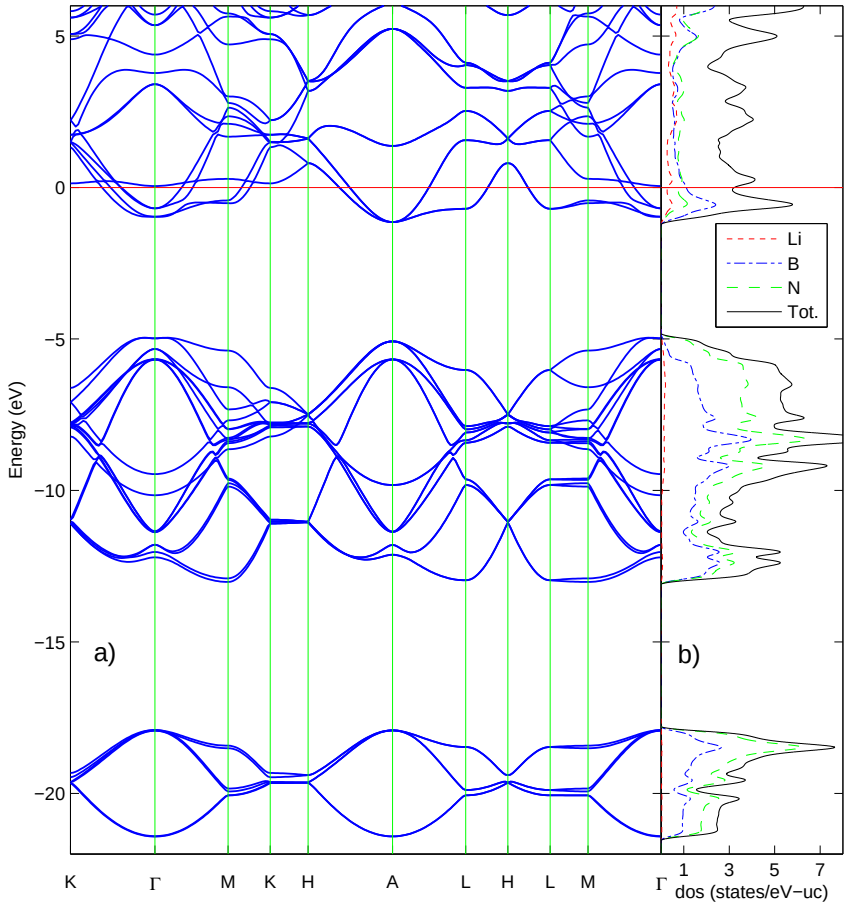

Figure 5.18: Band Structure and pdos of $(BN)_6Li_4$.

5.4.4 Interlayer States

Interlayer states are nearly free-electron like and exist in many layered-compounds, such as graphite and hBN and their nanotubes [104]. A DFT-LDA study by Margine and Crespi on the change of the position of the interlayer derived state in carbon nano-tubes indicate that the change is not due to the hybridization between the alkali *s* state and the interlayer state but due to a universal electrostatic mechanism. [105].

Near-edge x-ray absorption fine-structure (NEXAFS) measurements by Pacile *et. al.* on graphene confirmed the existence of an interlayer state even in single

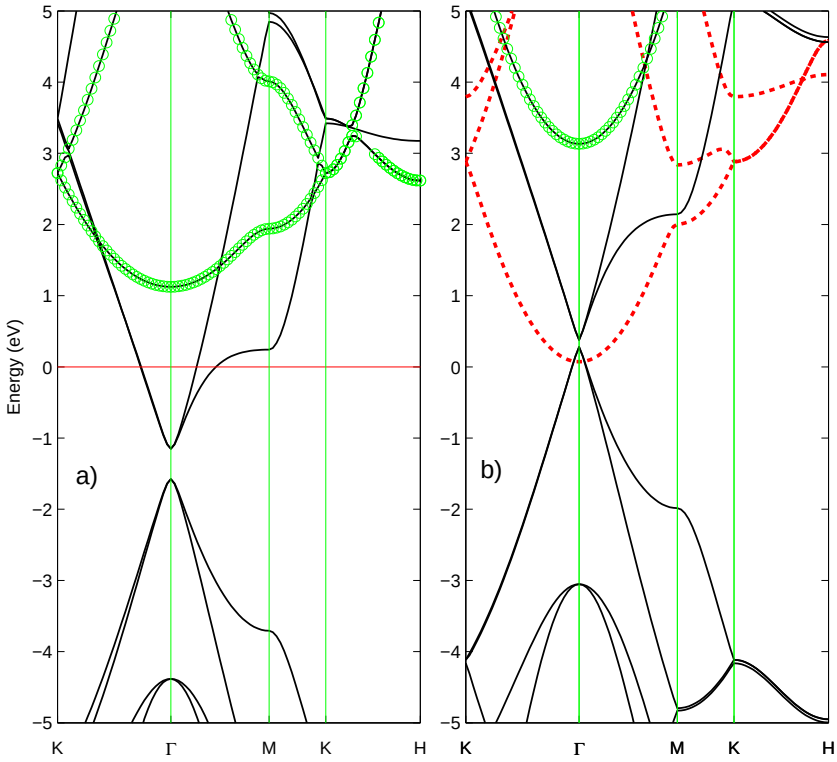

Figure 5.19: a) Band structure of C_6Li(interlayer state is indicated by dots). b) Band structure of Li(dotted red line) and C(straight line) in C_6Li structure, the interlayer state is again indicated by green dots.

layer graphite. [106]

Calandra and Mauri investigated the role of interlayer states in superconductivity of C_6Ca and found that the presence of superconductivity is dependent on the existence of an intercalant Fermi surface, so a noncomplete ionization of the intercalant is important in superconductivity [107].

On the other hand, Sugawara *et. al.* have used high resolution ARPES technique and found that the interlayer band is essential in explaining superconductivity in C_6Ca. [108].

We investigated the interlayer state in greater detail for C_6Li, C_3Li, $(BN)_3Li$

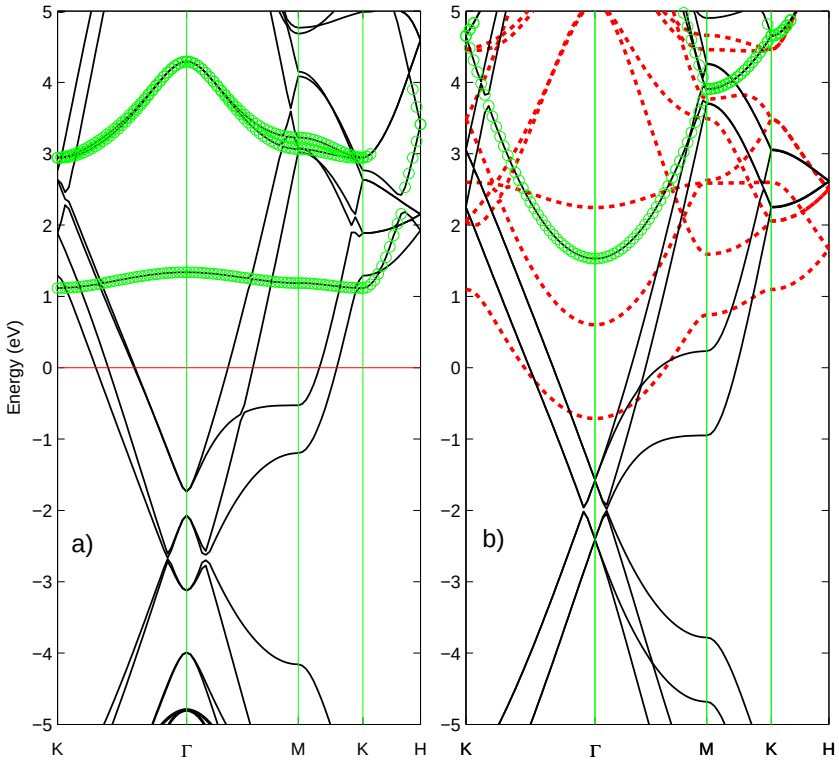

Figure 5.20: a) Band structure of C_3Li(interlayer state is indicated by dots). b) Band structure of Li(dotted red line) and C(straight line) in C_3Li structure, the interlayer state is again indicated by green dots.

and $(BN)_6Li_4$ and present the band structure near fermi level in Figures 5.20-5.22. In each of these figures, part a shows the band structure of the intercalated compound which part b shows the band structure of the same crystal with either C(BN) or Li taken out. In both parts the interlayer band is indicated.

One important result from these graphs is that the interlayer band is not occupied in C_6Li or C_3Li. Since C_3Li shows superconductivity of very low temperatures. This finding seem to negate the idea that for superconductivity of alkali-graphite intercalation compounds, interlayer state needs to be occupied.

Another important observation can be glanced from Figure 5.21, which shows

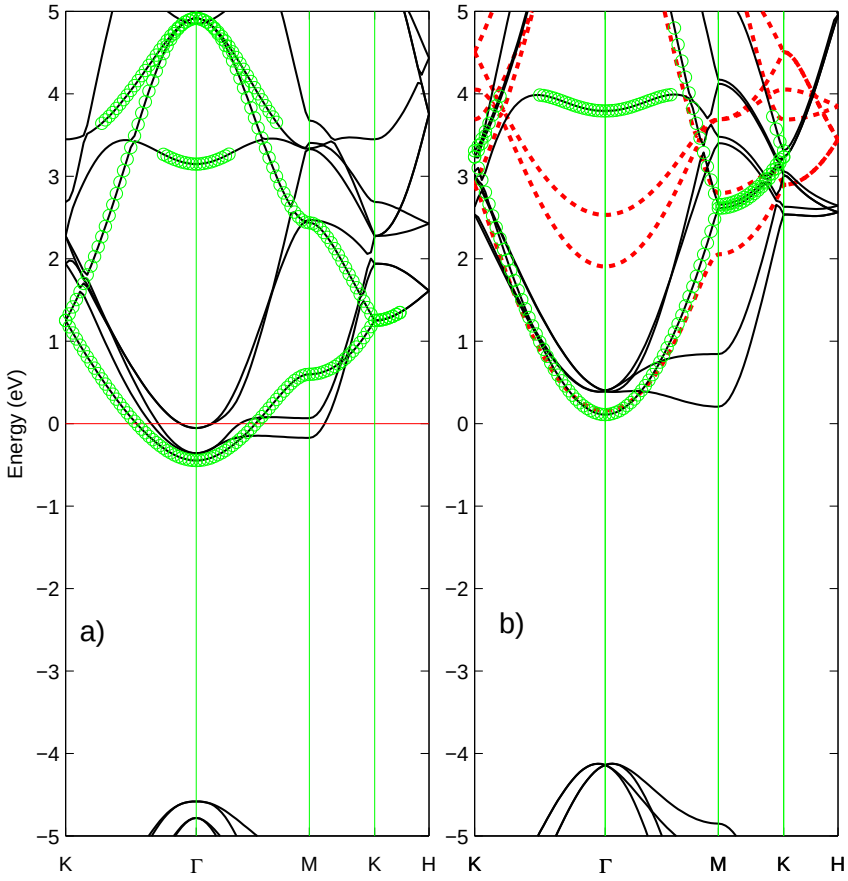

Figure 5.21: a)Band structure of $(BN)_3Li$(interlayer state is indicated by dots). b) Band structure of Li(dotted red line) and BN(straight line) in $(BN)_3Li$ structure, the interlayer state is again indicated by green dots.

that the interlayer state is well occupied for $(BN)_3$. If we add from Figure 5.16 that the density of states at E_F is very high ($n(E_F) \simeq 7$ states/eV) for $(BN)_3Li$ one would expect a relatively high superconducting temperature for $(BN)_3Li$ if interlayer state superconductivity relation is valid.

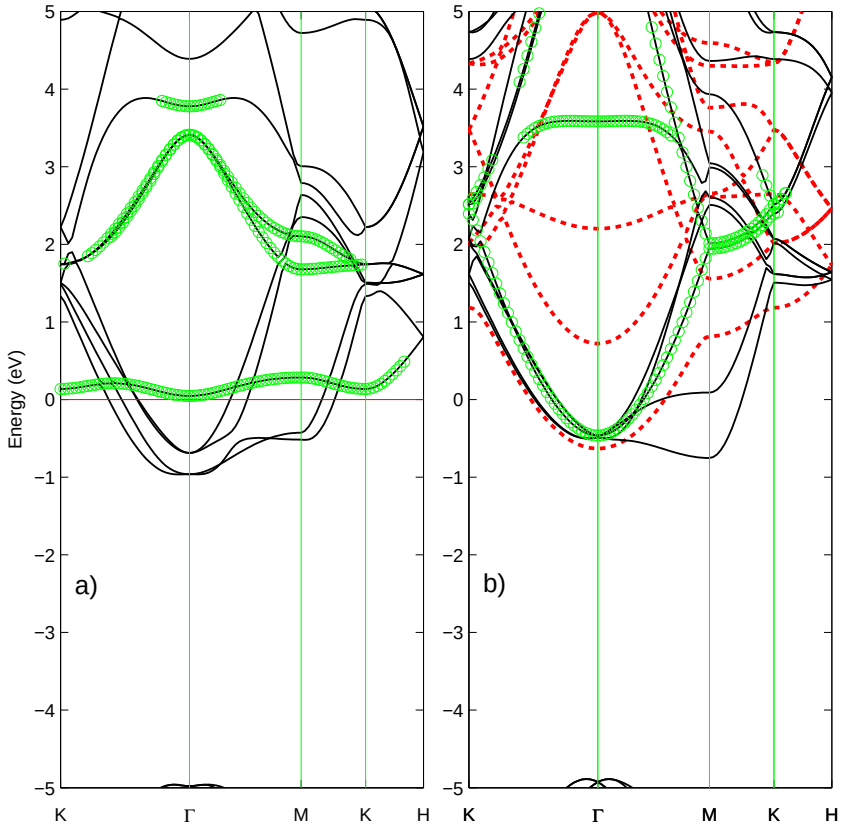

Figure 5.22: a)Band structure of $(BN)_6Li_4$(interlayer state is indicated by dots). b) Band structure of Li(dotted red line) and BN(straight line) in $(BN)_6Li_4$ structure, the interlayer state is again indicated by green dots.

5.4.5 Fermi Surface

The calculated Fermi surface of GICs and hBN intercalation compounds are shown in Fig. 5.23 for C_6Li and $(BN)_3Li$ and Fig. 5.24 for C_3Li and $(BN)_6Li_4$. The Fermi surface is made of three main parts, one around the Γ point in spherical shape, one along Γ-A direction cylindrical shape and sheet along Γ-M directions. The Fermi surface for both of the compounds are similar with slight differences.

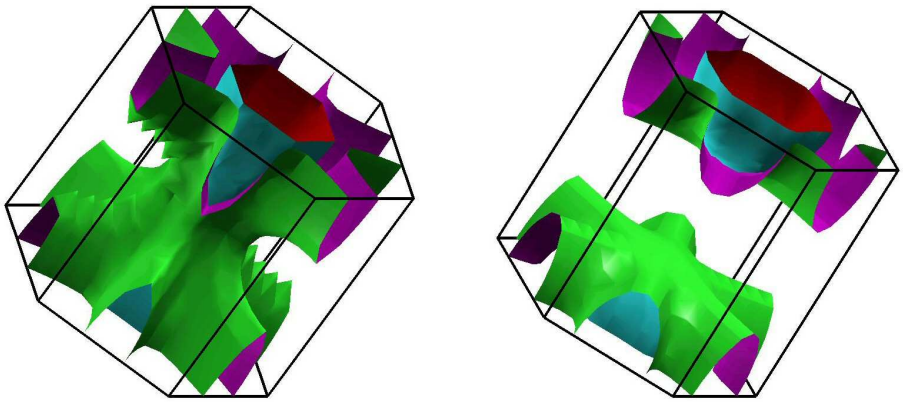

Figure 5.23: Fermi surfaces of C_6Li and $(BN)_3Li$.

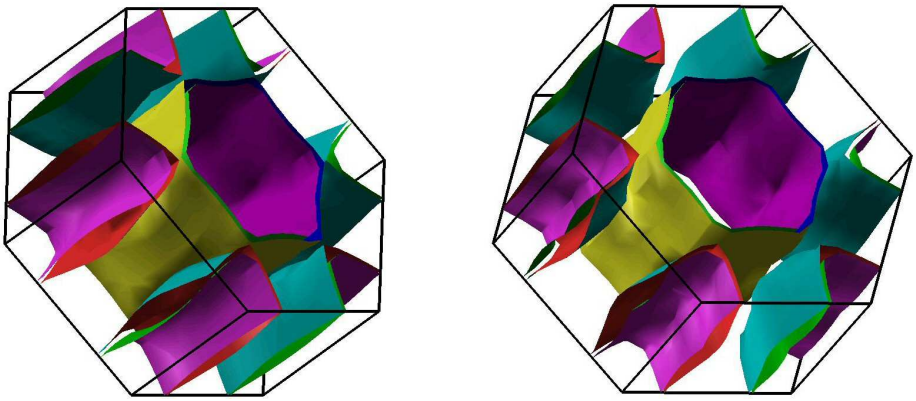

Figure 5.24: Fermi surfaces of C_3Li and $(BN)_6Li_4$.

CHAPTER 6
ALKALI INTERCALATION OF GRAPHITE AND HBN - ELASTIC AND LATTICE DYNAMICAL PROPERTIES

6.1 Phonon Studies

Pure graphite crystallizes according to the space group $D_{6h}{}^4$ (space group number 194 ($P6_3/mmc$)) with four atom per primitive unit cell and as a result has 12 phonon modes. Three of these modes of symmetry $A_{2u} \oplus E_{1u}$ are of a acoustic type and have zero frequency for zero wave vector,i.e. at the center of the first Brillouin zone. Three of the remaining nine modes ($A_{2u} \oplus E_{2u}$) are infrared active. Four 2 E_g symmetry are Raman active while 2 B_{1g} modes are silent, i.e. can not be measured by using optical spectroscopy techniques, can only be detected by using neutron spectroscopy. The phonon frequencies of graphite has been studied by many groups over the years by using Raman scattering[109], infrared spectroscopy and inelastic neutron scattering[110].

As the starting point of lattice dynamics of intercalated compounds of graphite and hBN, we have calculated the gamma point phonon modes of graphite and displayed it in Table 6.3. The calculations above are done by using linear response theory in the density functional theory framework. The electron-ion interactions are accounted for by using optimized pseudopotentials. The electronic wave functions are expanded in plane waves with a cutoff of 40 Ha and Brillouin zone integrations are approximated by using a 20 20 20 Monkhorst-Pack grid.

There are number of discrepancies between the model calculations and first principles calculations concerning the level crossings and shape of the lower frequency phonon branches, such ad the crossing of acoustic and optical branches near M point and energy of the acoustic modes at K point.

Another important property of phonon dispersion of graphite is the existence of Kohn anomaly for the highest frequency optical mode at the K point.

The first principles phonon calculations in the framework of density functional perturbation theory have been carried out by a number of groups[111, 112, 113, 114, 115, 116].

In graphite and diamond, the highest frequency optical mode is a a finite wave-vector which is due to the reduction of zone center mode frequency because of interaction of the mentioned mode with the electronic system. this effect is called overbending and results from a Kohn anomaly.

6.1.1 Elastic constants

Elastic constant is a quantity which gives the strain-stress relation for a crystal structure. There are 36 components of a elastic tensor but this components can be reduced to its independent components by using symmetry of the system.

For hexagonal structure (space groups numbers 176($(BN)_6Li_4$), 189($(BN)_3Li$,C_3Li), 191(C_6Li) and 194(Graphite and hBN) in our study), there are 5 independent elastic constants are available(C_{11}, C_{12}, C_{13}, C_{33}, C_{44}) and one extra elastic constant (C_{66}=(C_{11}-C_{12})/2) which derived from C_{11} and C_{12}.

The components of compliance tensors for graphite, hBN and their Li intercalated compound are given in Table 6.1 along with experimental and theoretical data.

Since our calculated elastic constants for hBN and graphite are in good agree-

ment with experimental data and previous DFT calculations, we can assume that the results for the intercalation compounds have comparable accuracy.

Our general observation from the Table 6.1 is that the components of C are lower for the intercalated compounds of graphite compared to those of pure graphite except for the off-diagonal (C_{13}, C_{33}, C_{44}) components. A similar trend is observed for hBN intercalation compounds except that the increasing components are C_{13}, C_{33}, C_{66}.

Table 6.1: Elastic Constants of graphite, hBN, C_6Li, $(BN)_3Li$, C_3Li and $(BN)_6Li_4$ in GPa

Compound	C_{11}	C_{12}	C_{13}	C_{33}	C_{44}	C_{66}
C_6Li	895.3	145.7	27.6	64.81	16.5	374.8
C_6Li,Theo.[117]	747			47.1	15	391
$(BN)_3Li$	768.9	187.9	12.4	74.4	33.4	290.5
C_3Li	883.6	148.9	-2.9	180.3	29.2	367.3
$(BN)_6Li_4$	800.6	169	32.0	78.7	-3.8	392.0
hBN	905	209	2.2	27	5	348
Graphite	1009.2	179.5	-3.4	20.6	-2.9	414.9
Graphite,Theo.[117]	1130		-	37.4	4.4	388
Graphite,Exp.[118, 119]	1060			36.5	4.0	440

6.1.2 Lattice dynamics

As first step of the investigation of lattice dynamical properties, we will consider the normal modes od the considered structures and discuss the displacement patterns for the representative zone center vibrational modes.

The displacement patterns for the zone center vibrational modes for C_6Li are shown in Figure 6.1 through Figure 6.4 for representative symmetries. The intercalant lithium atom is found to be in motion only for low frequency modes at 203 cm^{-1} and 449 cm^{-1}. for the mode #6, C layers move in z-direction as whole while Li atoms move in -z direction, while mode #5 involves Li and C layers moving in x-y plane opposite to each other.

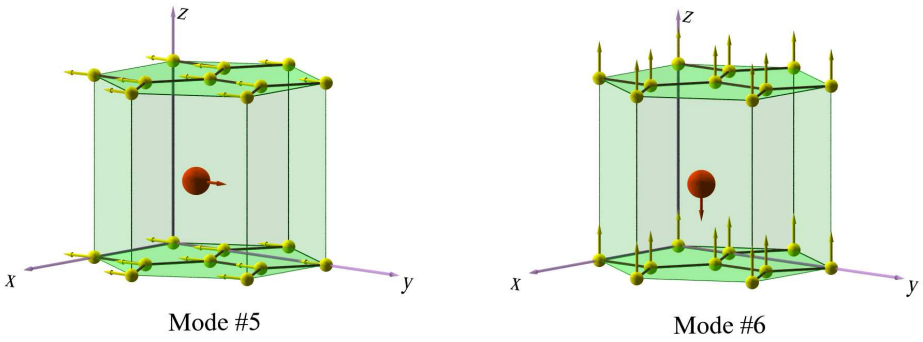

Figure 6.1: Displacement patterns of vibrational modes #5(ω=203 cm^{-1}) and #6(ω=449 cm^{-1}) for C_6Li.

Intermediate frequency modes (Figure 6.2) involve only motion of the carbon atoms in z-direction half of the atoms at the corners of the hexagons that make up the honeycomb lattice more up while the other half moves down. the weakness of the interlayer interaction is the reason for the vibrational frequency of these modes being lower compared to the modes that involve intralayer displacements.

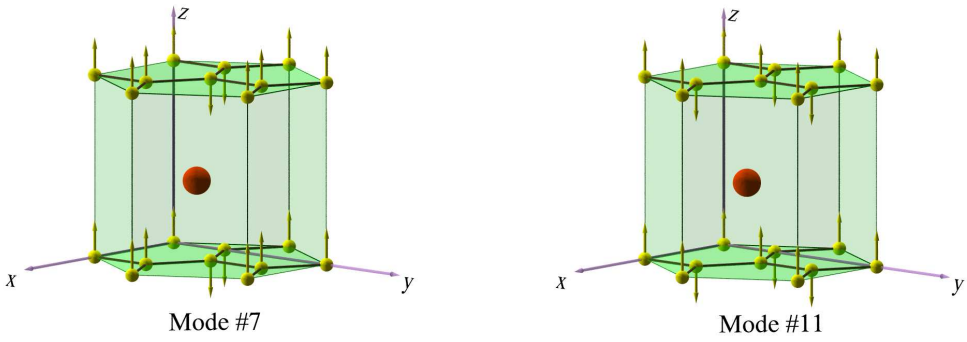

Figure 6.2: Displacement patterns of vibrational modes #7(ω=464 cm^{-1}) and #11(ω=805 cm^{-1}) for C_6Li.

The high frequency modes at the center of the Brillouin zone for C_6Li are displayed in Figure 6.3 through Figure 6.4 and involve mostly the displacement od carbon atoms on the two dimensional honeycomb lattice. These modes are mostly breathing type distortion of the hexagons and because of strong sp^2 type

covalent bonding in this plane their frequency is high.

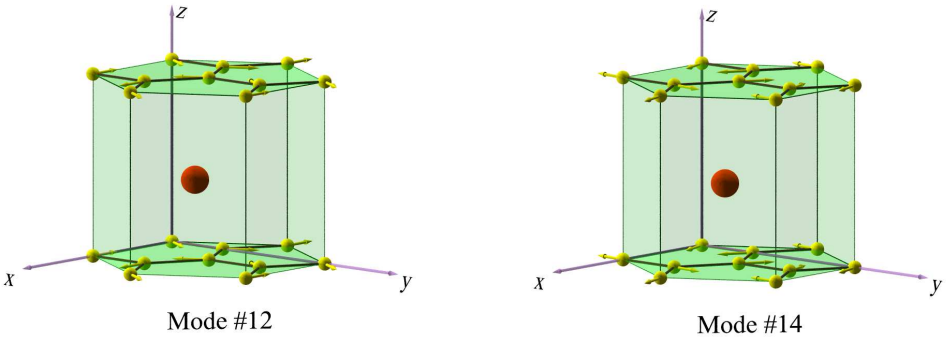

Figure 6.3: Displacement patterns of vibrational modes #12(ω=985 cm^{-1}) and #14(ω=1151 cm^{-1}) for C_6Li.

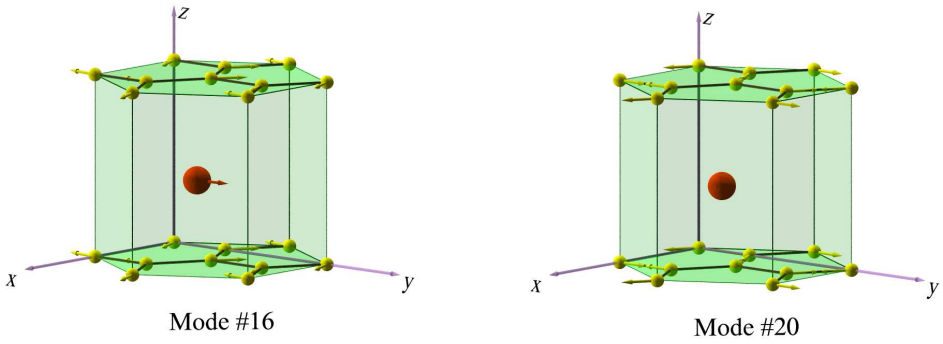

Figure 6.4: Displacement patterns of vibrational modes #16(ω=1178 cm^{-1}) and #20(ω=1421 cm^{-1}) for C_6Li.

The displacement patterns of the vibrational modes of $(BN)_3Li$ which is analogous to C_6Li are shown in Figure 6.5-Figure 6.8 for some representative symmetries. Because of the doubling of the primitive unit cell when going from C_6Li to $(BN)_3Li$, the displacement patterns are not easy to compare. the Most important overall difference in $(BN)_3Li$ ease seem to the lithium participation.

Mode #4 of C_3Li at 112 cm^{-1} involves adjacent layer moving against each other, since the interlayer interaction in weak the mode frequency low.

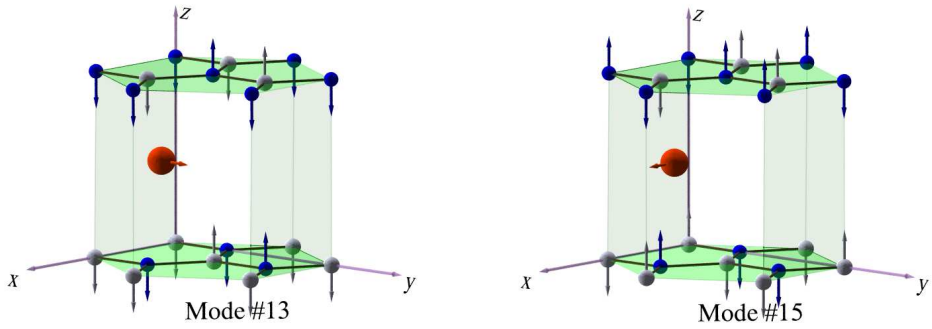

Figure 6.5: Displacement patterns of vibrational modes #13(ω=287 cm^{-1}) and #15(ω=302 cm^{-1}) for $(BN)_3Li$.

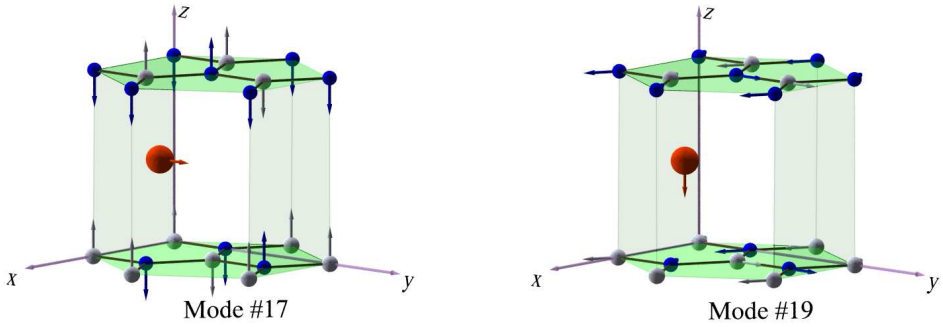

Figure 6.6: Displacement patterns of vibrational modes #17(ω=323 cm^{-1}) and #19(ω=354 cm^{-1}) for $(BN)_3Li$.

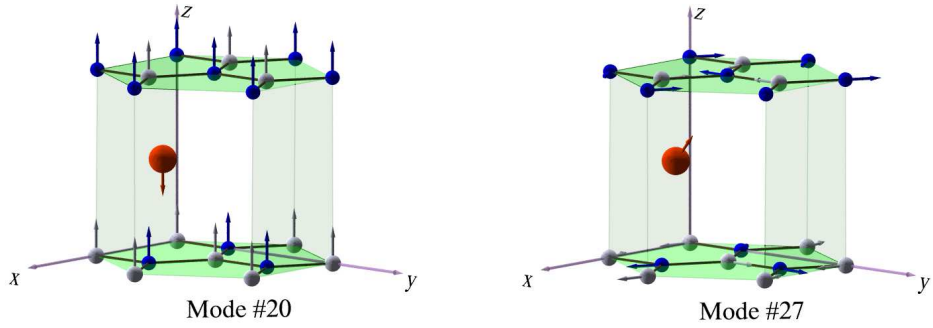

Figure 6.7: Displacement patterns of vibrational modes #20(ω=361 cm^{-1}) and #27(ω=975 cm^{-1}) for $(BN)_3Li$.

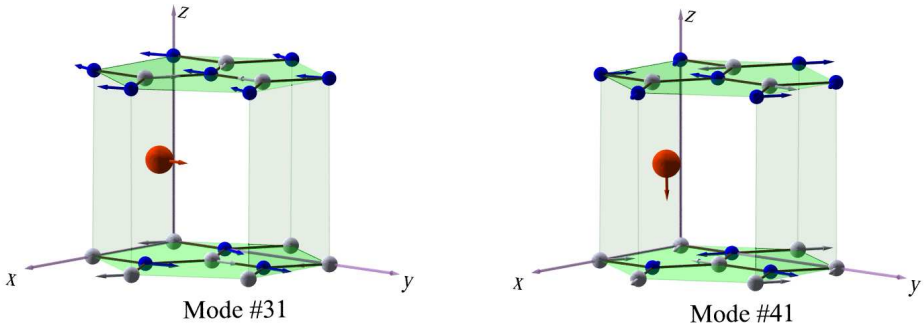

Figure 6.8: Displacement patterns of vibrational modes #31(ω=1128 cm^{-1}) and #41(ω=1302 cm^{-1}) for $(BN)_3Li$.

The displacement of intermediate frequency modes of C_3Li involve motion of carbon atoms in ±z directions.

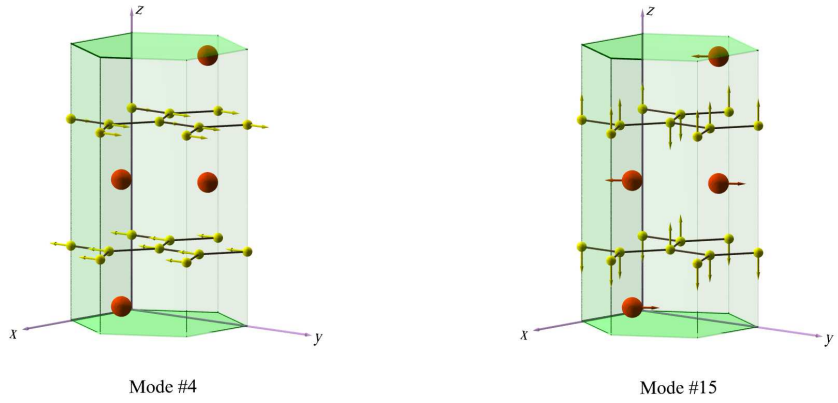

Figure 6.9: Displacement patterns of vibrational modes #4(ω=112 cm^{-1}) and #15(ω=396 cm^{-1}) for C_3Li.

High frequency modes of C_3Li also involve motion of carbon atoms in the hexagon against each other, similar to the case for C_6Li and their high frequency reflect the interlayer strong sp^2 covalent bonding.

Negative frequency modes (Mode #1 and Mode #3) of $(BN)_6Li_4$ involves that the direction of the motion of boron and nitrogen atoms in ±z direction while Lithium atoms moves along xy plane of the unit cell.

Mode #19 and Mode #26 at midrange(343 cm^{-1} and 417 cm^{-1}) frequencies

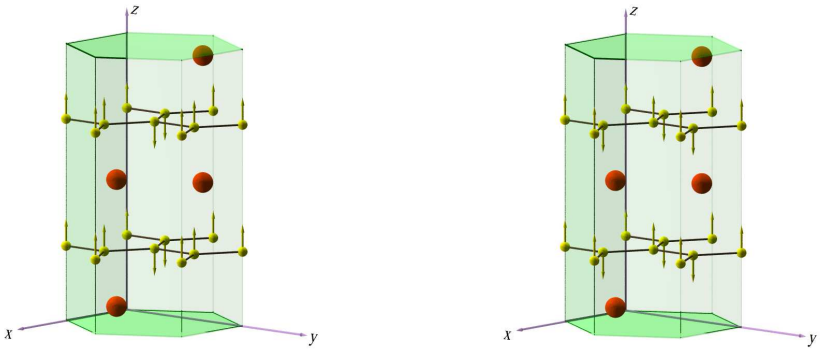

Figure 6.10: Displacement patterns of vibrational modes #22(ω=444 cm^{-1}) and #28(ω=617 cm^{-1}) for C_3Li.

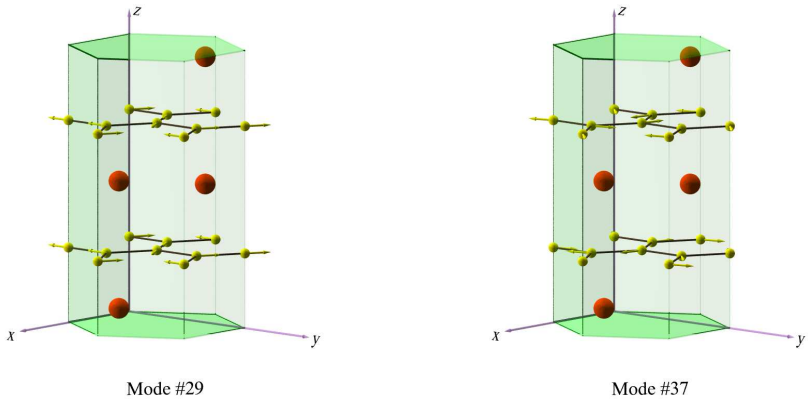

Figure 6.11: Displacement patterns of vibrational modes #29(ω=961 cm^{-1}) and #37(ω=1077 cm^{-1}) for C_3Li.

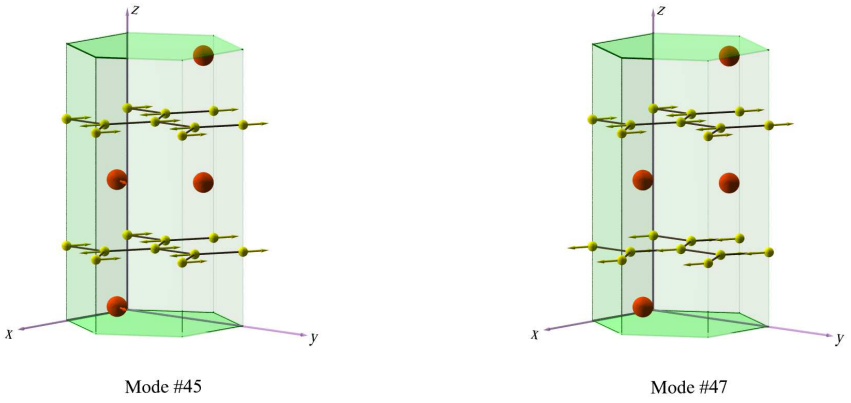

Figure 6.12: Displacement patterns of vibrational modes #45(ω=1475 cm^{-1}) and #47(ω=1501 cm^{-1}) for C_3Li.

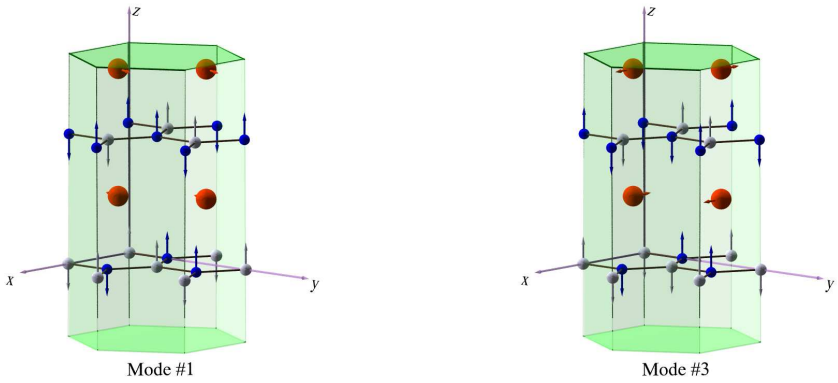

Figure 6.13: Displacement patterns of vibrational modes #1(ω=-404 cm^{-1}) and #3(ω=-352 cm^{-1}) for $(BN)_6Li_4$.

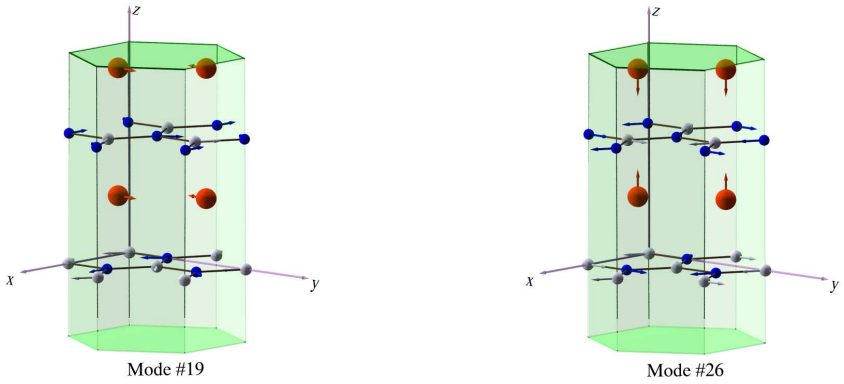

Figure 6.14: Displacement patterns of vibrational modes #19(ω=343 cm^{-1}) and #26(ω=417 cm^{-1}) for $(BN)_6Li_4$.

and involve that motion of the boron and nitrogen atoms in hexagons is opposite direction on xy plane and motion of the Lithium is in xy plane in Mode #19 and z-direction in Mode #26.

Higher frequency modes of $(BN)_6Li_4$ over 1000 cm^{-1} involves displacement of boron and nitrogen atoms on the layer are on xy plane.

6.1.3 Phonon Dispersions

The phonon dispersions along the K-Γ-M-K-H-A-L-H-L-M-Γ-A high symmetry directions for all the intercalation compounds analyzed in this section have been

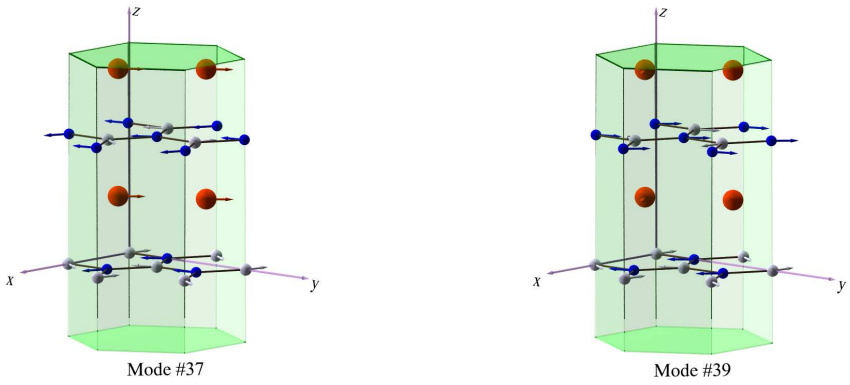

Figure 6.15: Displacement patterns of vibrational modes #37(ω=1044 cm^{-1}) and #39(ω=1049 cm^{-1}) for $(BN)_6Li_4$.

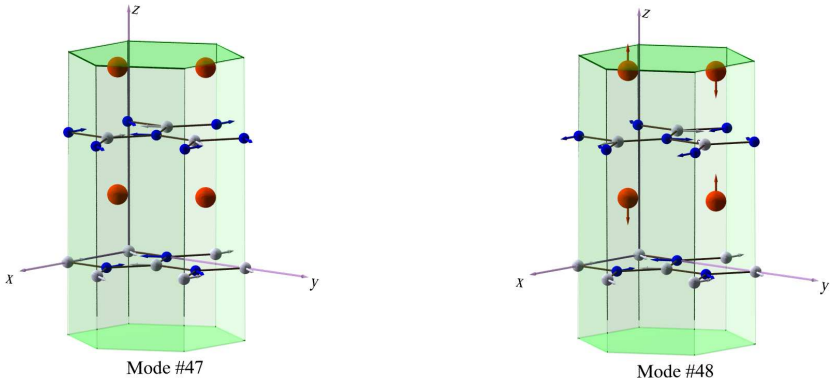

Figure 6.16: Displacement patterns of vibrational modes #47(ω=1256 cm^{-1}) and #48(ω=1261 cm^{-1}) for $(BN)_6Li_4$.

calculated and presented in Figures 6.18-6.21. As a test of the computational parameters we have calculated the phonon dispersions of pure hBN and also zone center vibrational frequencies of pure hBN and graphite and display the results along with experimental data of Ref.[120, 121, 122] and theoretical work of Ref.[123] in Figure 6.17 and Table 6.2,Table 6.3 for hBN and graphite respectively.

Table 6.2: Zone-center phonon modes of hBN in cm^{-1}

0	0	0	49	49
112	755	815	1391	1391
1391	1391			

As can be seen from the figure, the agreement between our calculation and

Table 6.3: Zone-center phonon modes of Graphite in cm^{-1}

0	0	0	43.3	43.3
107.3	901.3	905.8	1607.8	1607.8
1617.2	1617.2			

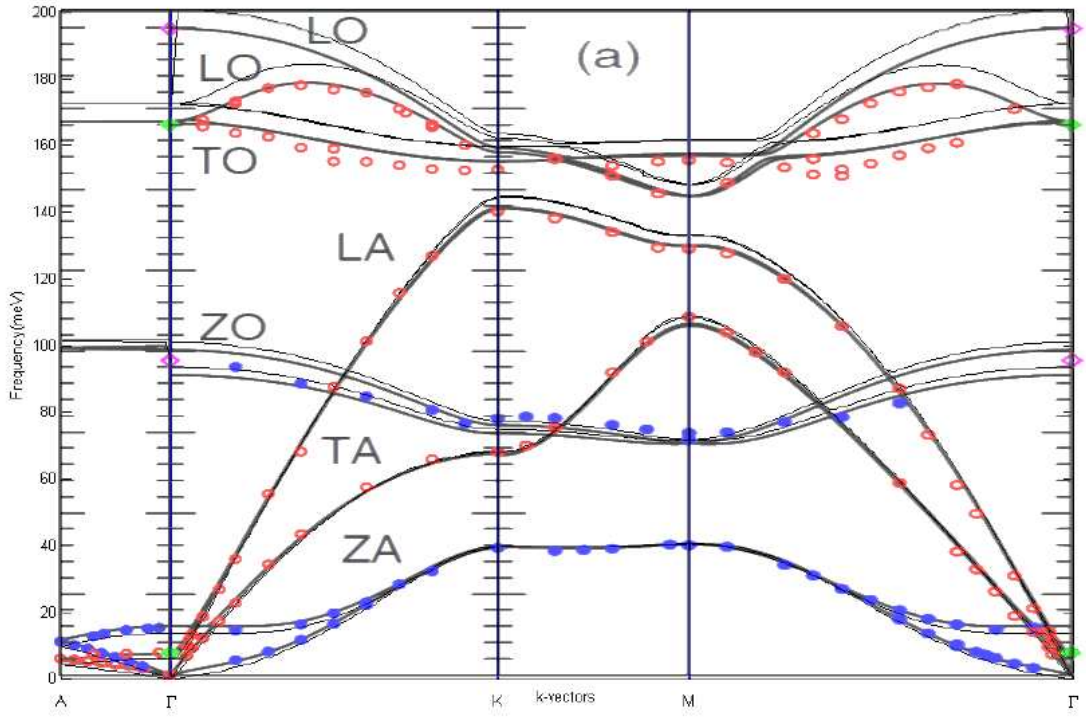

Figure 6.17: Phonon dispersion plot pristine hBN overlayed with inelastic x-ray scattering result and ab initio calculations of Bosak et. al.[123](our plot in thin lines)

the experiments is fair so we expect the dispersions for the similar intercalated system to be on the order of same level.

In Figure 6.19 we displayed the C_6Li phonon dispersion merged with literature data[112] along A-Γ-M high symmetry directions and in Figure 6.18 we displayed the phonon dispersion and atom projected density of states for C_6Li. The dispersion plot can be understood as three basic bands of high, intermediate and low frequency vibrations. As it also has been indicated in the previous section, the high frequency bands are due to vibrations of carbon atoms in the 2D hon-

eycombs lattice which are high frequency due to the bands being strong sp^2 type on this plane. The intercalant modes are very visible from the projected phonon density of states around 30 and 60 meV and they are almost dispersionless bands, i.e. their energy does not depend on the wave-vector.

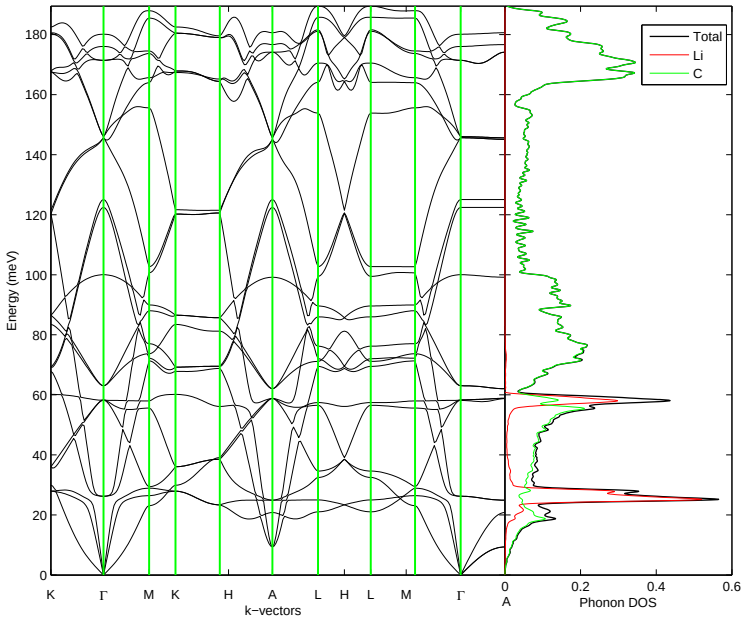

Figure 6.18: Phonon dispersion plot for C_6Li along with phonon density of states plot.

The vibrational bands of C_6Li analogue of hBN are shown in Figure 6.20. The overall structure is similar to that of C_6Li but a very prominent difference is the existence of a negative frequency band along H-A-L-H-L which indictaes that $(BN)_3Li$ is dynamically unstable,i.e. the vibrations along z-axis would disintegrate the compound.

Figure 6.21 similarly displays the dispersion of phonons in C_3Li along the same directions as Figure 6.18 and atom projected phonon density of states. Again, the intercalant bands are at low frequencies and show dispersion which means that they do not interact strongly with the intercalant lattice.

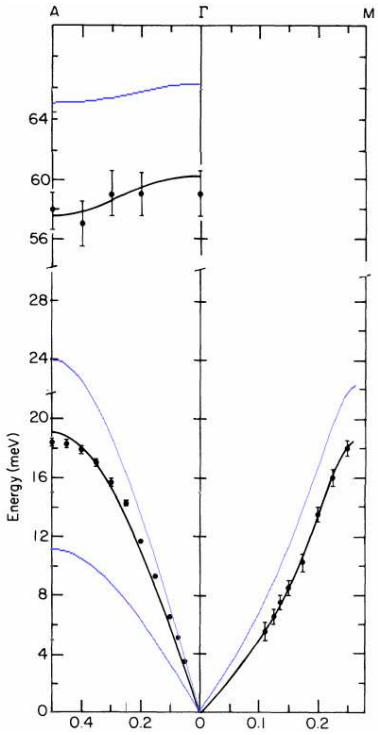

Figure 6.19: C_6Li phonon dispersion merged with literature data.[112]

For the hBN analogue of C_3Li (i.e. $(BN)_6Li_4$), we were not be able to obtain a stable phonon dispersion. So we have calculated its zone center vibrational frequencies and display them in Table 6.4. As can be seen from the table, $(BN)_6Li_4$ is also dynamically unstable, because some of the modes have negative frequencies.

Table 6.4: Zone-center phonon modes of $(BN)_6Li_4$ in cm^{-1}

-404	-404	-352	-352	-57	-57
0	0	0	138	146	146
152	152	310	310	334	334
343	343	343	383	391	391
409	417	424	446	798	808
836	846	868	868	869	869
1044	1044	1049	1049	1190	1190
1197	1197	1208	1212	1256	1261

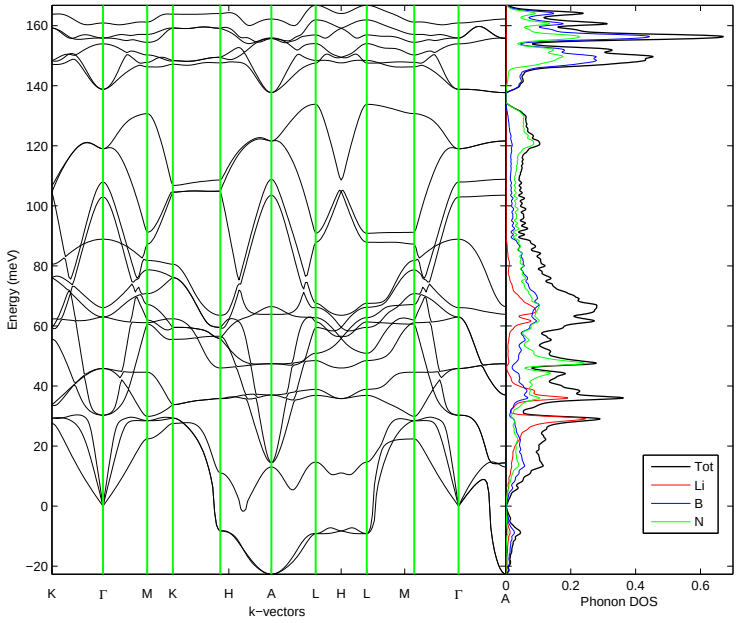

Figure 6.20: Phonon dispersion plot for $(BN)_3Li$ along with phonon density of states plot.

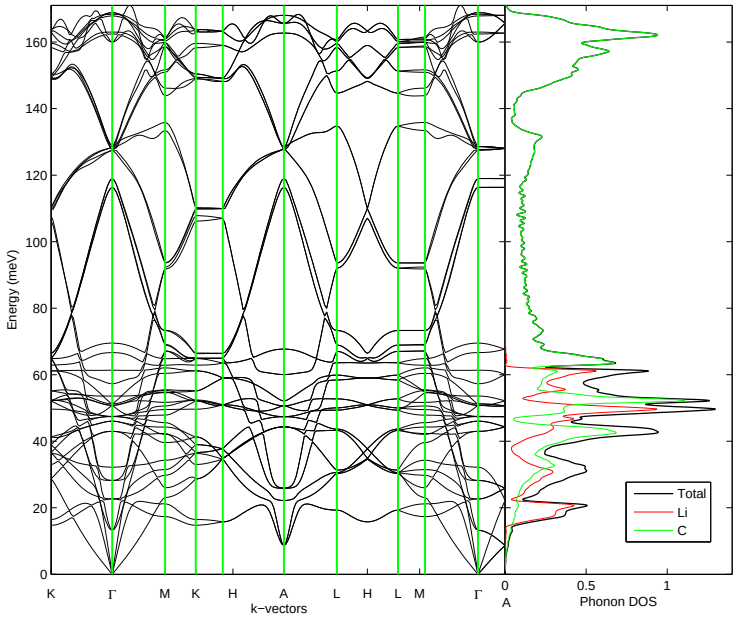

Figure 6.21: Phonon dispersion plot for C_3Li along with phonon density of states plot.

CHAPTER 7
CALCIUM INTERCALATION INTO GRAPHITE AND HBN

7.1 Introduction

Graphite intercalation compounds are very important and there are hundreds of intercalation compound of graphite reported. The most popular intercalation product of graphite is calcium intercalated form because of its superconducting property. Calcium intercalated graphite show superconductivity at 11.5 ^{o}K and this is widely explained by some groups[95, 107, 124].

While there are many studies on calcium intercalation into graphite, there is no any study reported for calcium-hBN intercalation.

Here we report the structural, electronic, and lattice dynamical properties of calcium intercalation into hBN and compare between its graphite analogue C_6Ca.

7.2 Computational Details

For the calculation of calcium intercalated graphite and hBN, we used the same pseudopotentials for Carbon, Boron and Nitrogen as in described in previous chapter. For calcium atom pseudopotentials were generated for $3s^2$ $3p^6$ $3d^0$ $4s^2$ valance configuration and cut-off radius were taken as 1.42, 1.72, 1.80, 1.74 for 3s, 3p, 3d, 4s orbitals. The exchange correlation energy is evaluated in local density approximation(LDA), using Perdew-Wang parametrization[39] of Ceperley-Alder electron-gas data[40].

For C_6Ca calculation, Monkhorst-Pack grid was chosen as 8 8 8 and at energy cut off 40 Ha and for $(BN)_3Ca$ calculations, 6 6 4 Monkhorst-Pack grid used at energy cut off 40 Ha.

7.3 Results

7.3.1 Structural Properties

The structural parameters calculated for C_6Ca are similar to the results reported previously by Mazin[95]. The C_6Ca system crystallizes in rhombohedral structure which is described by a lattice constant a and the angle α between any two of the lattice vectors. Our calculated lattice parameters, a, α, the bond lengths C-C, C-Ca, B-N, B-Ca and N-Ca are shown in Table 7.1 along with the experimental data.

Table 7.1: Calculated lattice parameters and bond lengths for C_6Ca and $(BN)_3Ca$

C_6Ca			$(BN)_3Ca$	
	This work	Experimental[125]		
a	9.6485 Bohr	9.7698 Bohr	**a**	9.8611 Bohr
α	50.66 Degree	49.55 Degree	α	47.56 Degree
C-C	2.7455 Bohr	2.7303 Bohr	**B-N**	2.76424 Bohr
Ca-C	5.0157 Bohr	5.0769 Bohr	**Ca-B**	5.3316 Bohr
			Ca-N	5.3227 Bohr

As can be seen in the table, there is a good agreement between the calculated and the measured quantities. The structural optimization of Ca intercalated h-BN does not indicate any instability, i.e. there exists at least a quasi-equilibrium Ca intercalated hBN according to these results.

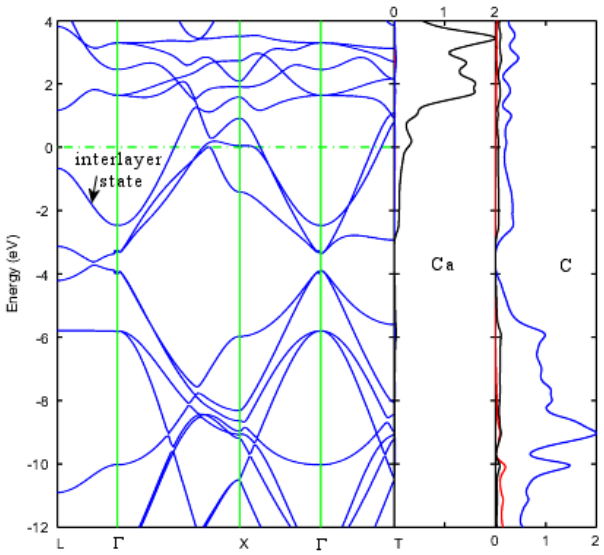

Figure 7.1: a) C_6Ca band structure, b) and c) electronic partial density of states, PDOS plots for Ca and C respectively. In PDOS plots red, blue and black lines represent s, p and d states.

7.3.2 Electronic Properties

Under this topic I have investigated the band structure, local density of states and the Fermi surface of C_6Ca, $(BN)_3Ca$ and pristine $(BN)_3$ in the rhombohedral structure. Since, C_6Ca has a relatively high superconducting transition temperature at 11.5 ^oK, it has been the subject of many theoretical and experimental study, recently. One interesting point in these studies is the claimed to due to the interaction of an interlayer-state and alkali s-states with phonons.

The calculated band structure for C_6Ca, $(BN)_3Ca$ and pristine $(BN)_3$ in rhombohedral phase are shown in Figure 7.2, 7.2 and 7.3 respectively. As expected, rhombohedral graphite is found to be semi-metal with a near-zero forbidden gap, while rhombohedral $(BN)_3$ is a wide-gap semiconductor or insulator. The effect of alkali intercalation can bee seen from the Figures 7.2 and 7.2; both system become metallic which is displayed by Fermi-level cutting of the bands.

The Fermi surface of a metallic system shows the constant energy surface that

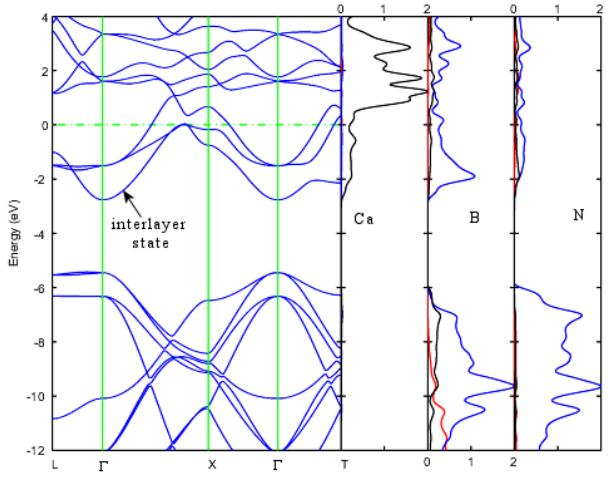

Figure 7.2: a) $(BN)_3Ca$ band structure, b), c) and d) electronic partial density of states, PDOS plots for Ca, B and N respectively. In PDOS plots red, blue and black lines represent s, p and d states.

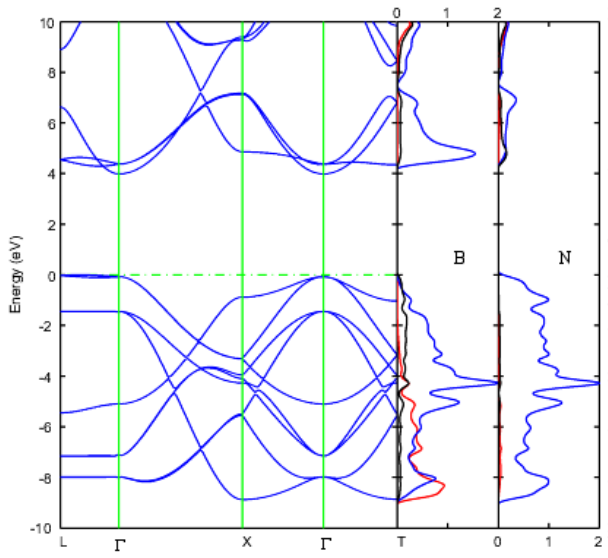

Figure 7.3: a) $(BN)_3$ band structure, b) and c) electronic partial density of states, PDOS plots for B and N respectively. In PDOS plots red, blue and black lines represent s, p and d states.

is occupied by the electrons at 0 ^{o}K. It is an important concept in conduction studies, because only the electrons very near this surface can take part in the electronic conduction. I have calculated Fermi surface of both C_6Ca and $(BN)_3Ca$ and show the result in Figure 7.4 and Figure 7.5 respectively. As it also can be seen from the band structure plots, the Fermi-level cuts through 3 of the bands and as a result Fermi surface has 3 structures. These directions are ΓX, XΓ, and ΓT of the Brillouin zone. Again our Fermi surface is in good agreement for C_6Ca with the one reported by Mauri et. al [126]

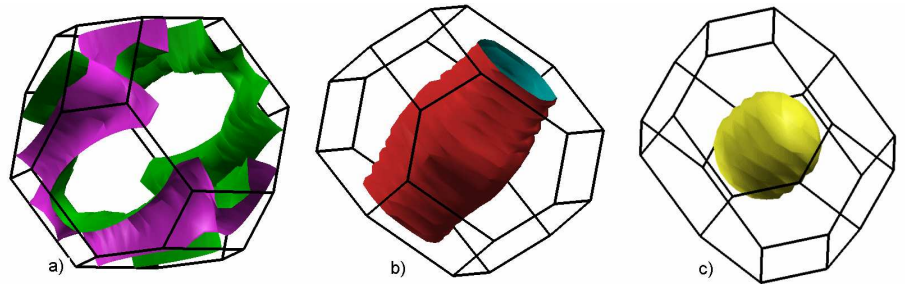

Figure 7.4: Fermi surface of C_6Ca. a-c) are contributions from the bands intercepts the fermi surface in Figure 7.1.

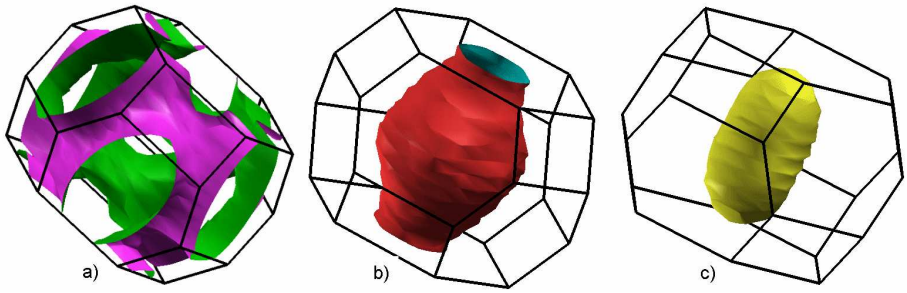

Figure 7.5: Fermi surface of $(BN)_3Ca$. a-c) are contributions from bands intercepts the fermi surface in Figure 7.2.

Furthermore, we have found another similarity between the electronic structure of C_6Ca and $(BN)_3Ca$. The interlayer state which is nearly free-electron like also exists for the $(BN)_3Ca$ system is shown in Figure 7.2 and corroborated by an examination of the wavefunctions.

7.3.3 Elastic and Lattice Dynamical Properties

Lattice dynamical properties give important clues on the bonding in the material. In this section I have calculated elastic compliance constants of C_6Ca, graphite, $(BN)_3Ca$ and rhombohedral $(BN)_3Ca$ for comparison purposes. Elastic compliance is a tensor quantity that describes the stress developed in a crystal in response to an applied strain and can be calculated as the second derivative of the total energy with respect to strain in two directions in the linear response framework. Our calculated compliance constants for C_6Ca and $(BN)_3Ca$ are displayed in Table 7.2 and calculated compliance constants for hbN and graphite are given in Table 7.3 with theoretical and experimental data. To give an indication of the quality of computational method, we also show the calculations of these quantities for graphite and hBN for which experimental data exists.

Table 7.2: Calculated elastic constants of C_6Ca and $(BN)_3Ca$ compared to experimental and theoretical data.

	$(BN)_3Ca$	C_6Ca	
	This Work	This Work	Theo.[117]
C_{11}	600	689	1340
C_{12}	130	86	
C_{13}	37	49	
C_{33}	78	115	150
C_{14}	5.5	4.3	
C_{44}	24	19	10.5
C_{66}	234	302	460

Compliance tensors are second-rank tensors with 36 components. The number of independent and non-zero element of the tensor is determined by the symmetries of the point group of the crystal system. For the rhombohedral structure considered here the point group is D_{3d} and has six independent components. The difference between our calculated $C_{i,j}$ and experimental values is around 20 % at most which indicates that the similar order of magnitude errors exist also for the

Table 7.3: Calculated elastic constants of hBN and graphite compared to experimental and theoretical data.

	hBN			Graphite		
	T.W.	Exp.[127]	Theo.[128, 129]	T.W.	Exp.[50]	Theo.[130, 47]
C_{11}	905	811	951.5,802	1009.2	1109	-,1440
C_{12}	209	169	169.2,267.5	179.5	139	-,-
C_{13}	2.2	0	2.5,3.0	-3.4	0	-0.5,-
C_{33}	27	27	28.2,31.2	20.6	38.7	40.8,37.1
C_{44}	5	7.7	-,3.0	-2.9	5.0	-,4.6
C_{66}	348			414.9	485	-,460

T.W.:This Work

values calculated for C_6Ca and $(BN)_3Ca$.

On this part, I have calculated the phonon dispersion relations for C_6Ca and $(BN)_3Ca$ along the high symmetry directions of the rhombohedral Brillouin zone and display the results in Figure 7.6 and 7.7 respectively. These dispersions, basically, show the vibration frequencies of the ion when their displacement pattern is one of the normal modes of the lattice with respect to the phonon momentum. As the unit cell has 7 atom, there are total 3*7=21 normal modes which represent the different displacement patterns. Normally, 3 of these modes are called "acoustic modes" that would have zero frequency at the center of the Brillouin zone; i.e. they correspond to linear translation of all the atoms in the unit cell, while the remaining modes are optical modes which would have positive frequencies along the whole of the Brillouin zone for a stable crystal. Phonon dispersions of C_6Ca have been studied by a number of groups, theoretically and experimentally, partly because electron-phonon interaction is the responsible factor for the superconductivity. Our calculated dispersion diagram for C_6Ca (Figure 7.6), is in good agreement with the other theoretical[126] and experimental work.

We have calculated the phonon dispersions of C_6Ca and $Ca(BN)_3$ and display the results in Figure 7.6 and 7.7.

The phonon dispersions of $(BN)_3Ca$ (Figure 7.7) show that there exists a neg-

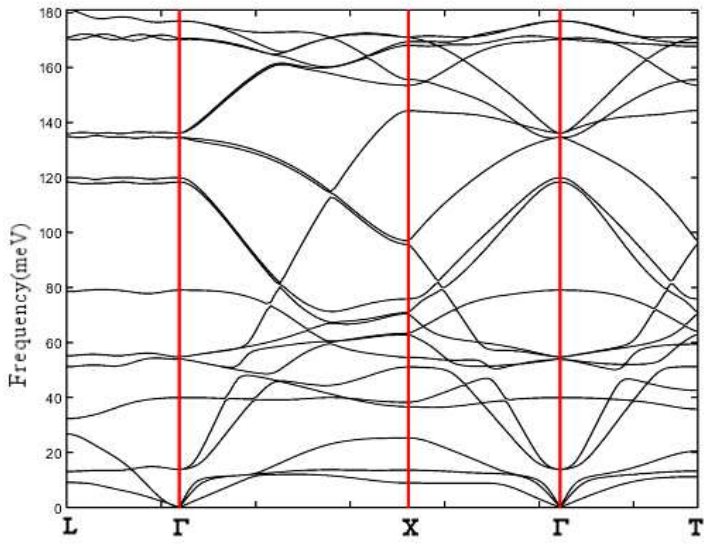

Figure 7.6: C_6Ca Phonon dispersions

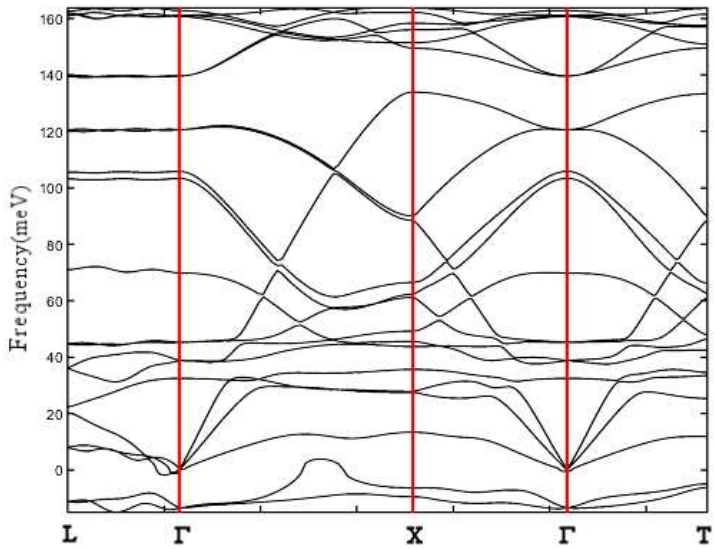

Figure 7.7: $Ca(BN)_3$ Phonon dispersions

ative frequency branch which is an indication of the instability of Ca-intercalated BN. So, based on the first principles calculations, we can speculate that the dynamical instability is the source of the difficulty of intercalating hBN with alkali metals.

REFERENCES

[1] Hohenberg, P. and Kohn, W. 1964, Inhomogeneous Electron Gas, *Phys. Rev.* **136**, B864-B871.

[2] Kohn, W. and Sham, L. J. 1965, Self-Consistent Equations Including Exchange and Correlation Effects, *Phys. Rev.* **140**, A1133-A1138.

[3] J. Ihm, e. a. 1980, Momentum-space formalism for the total energy of solids, *Journal of Physics C: Solid State Physics* **13**, 3095.

[4] Ascroft, N. W. and Mermin, N. D., 1975, *Solid State Physics*, Saunders College Publishing.

[5] Press, W. H., Teukolsky, S. A., Vetterling, W. T. and Flannery, B. P., 1988, *Numerical Recipes in C*, Cambridge University Press.

[6] Payne, M. C., Teter, M. P., Allan, D. C., Arias, T. A. and Joannopoulos, J. D. 1992, Iterative minimization techniques for ab initio total-energy calculations: molecular dynamics and conjugate gradients, *Rev. Mod. Phys.* **64**, 1045-1097.

[7] Yin, M. T. and Cohen, M. L. 1982, Theory of lattice-dynamical properties of solids: Application to Si and Ge, *Phys. Rev. B* **26**, 3259-3272.

[8] Baroni, S., Giannozzi, P. and Testa, A. 1987, Green's-function approach to linear response in solids, *Phys. Rev. Lett.* **58**, 1861-1864.

[9] Baroni, S., de Gironcoli, S., Dal Corso, A. and Giannozzi, P. 2001, Phonons and related crystal properties from density-functional perturbation theory, *Rev. Mod. Phys.* **73**, 515-562.

[10] Gonze, X. 1995, Perturbation expansion of variational principles at arbitrary order, *Phys. Rev. A* **52**, 1086-1095.

[11] Gonze, X. 1995, Adiabatic density-functional perturbation theory, *Phys. Rev. A* **52**, 1096-1114.

[12] Gonze, X. 1997, First-principles responses of solids to atomic displacements and homogeneous electric fields: Implementation of a conjugate-gradient algorithm, *Phys. Rev. B* **55**, 10337-10354.

[13] Gonze, X. and Lee, C. 1997, Dynamical matrices, Born effective charges, dielectric permittivity tensors, and interatomic force constants from density-functional perturbation theory, *Phys. Rev. B* **55**, 10355-10368.

[14] Griffiths, D., 2005, *Introduction to Quantum Mechanics*, Prentice Hall.

[15] Sakurai, J. J., 1994, *Modern Quantum Mechanics*, Addison-Wesley Publishing Company, Reading, MA, Revised edition.

[16] M. Hubácek, T. Sato, M. U. 1997, Copper-boron nitride interaction in hot-pressed ceramics, *J. Mater.Res.* **12**, 113-118.

[17] Hubácek, M. and Ueki, M. 1996, Orientation and Grain Growth in Copper-Activated Hot-Pressed Hexagonal Boron Nitride, *J. Am. Ceram. Soc.* **79**, 283-285.

[18] Budak, E. and Çetin Bozkurt 2004, The effect of transition metals on the structure of h-BN intercalation compounds, *Journal of Solid State Chemistry* **177**, 1768 - 1770.

[19] Dai, B. Q. and Zhang, G. L. 2002, Ab initio MO studies on the stability of intercalation compound Cu-hBN, *Materials Chem. Phys.* **77**, 318-320.

[20] Wirtz, L., Rubio, A., de la Concha, R. A. and Loiseau, A. 2003, Ab initio calculations of the lattice dynamics of boron nitride nanotubes, *Phys. Rev. B* **68**, 045425.

[21] Boehm, H. P., Setton, R. and Stumpp, E. 1994, Nomenclature and Terminology of Graphite Intercalation Compounds, *Pure & Appl. Chem.* **66**, 1893–1901.

[22] Dresselhaus, M. S. and G., D. 2002, Intercalation compounds of graphite, *Advances in Physics* **51**, 1-186.

[23] Dahn, J., Zheng, T., Liu, Y. and Xue, J. S. 1995, Mechanisms for Lithium Insertion in Carbonaceous Materials, *Science* **270**.

[24] Weller, T., Ellerby, M., S., S., Smith, R. and Skipper, N. 2005, Superconductivity in the intercalated graphite compounds C_6Yb and C_6Ca, *Nat. Phys.* **1**.

[25] Rey, N., Toulemonde, P., Machon, D., Duclaux, L., Floch, S. L., Pischedda, V., Itié, J. P., Flank, A.-M., Lagarde, P., Crichton, W. A., Mezouar, M., Strässle, T., Sheptyakov, D., Montagnac, G. and San-Miguel, A. 2008, High-pressure behavior of CsC_8 graphite intercalation compound: Lattice structures and phase-transition mechanism, *Physical Review B (Condensed Matter and Materials Physics)* **77**, 125433.

[26] Alexandre, S. S., Nunes, R. W. and Chacham, H. 2002, Energetics of the formation of dimers and solids of boron nitride fullerenes, *Phys. Rev. B* **66**, 085406.

[27] Dai, B. Q. and Zhang, G. L. 2003, A DFT study of hBN compared with graphite in forming alkali metal intercalation compounds, *Materials Chem. Phys.* **78**, 304-307.

[28] Shen, C., Mayorga, S. G., Biagioni, R., Piskoti, C., Ishigami, M., Zettl, A. and Bartlett, N. 1999, Intercalation of Hexagonal Boron Nitride by Strong Oxidizers and Evidence for the Metallic Nature of the Products,, *Journal of Solid State Chemistry* **147**, 74 - 81.

[29] Ritsko, J. J. 1982, Valence- and core-electronic excitations in potassium-intercalated graphite, *Phys. Rev. B* **25**, 6452-6459.

[30] Sun, G., Kertesz, M., Kürti, J. O. and Baughman, R. H. 2003, Dimensional change as a function of charge injection in graphite intercalation compounds: A density functional theory study, *Phys. Rev. B* **68**, 125411.

[31] Holzwarth, N. A. W., Louie, S. G. and Rabii, S. 1982, X-ray form factors and the electronic structure of graphite, *Phys. Rev. B* **26**, 5382-5390.

[32] Hightower, A., Ahn, C. C., Fultz, B. and Rez, P. 2000, Electron energy-loss spectrometry on lithiated graphite, *Appl. Phys. Lett.* **77**, 238-240.

[33] Bindra, C., Nalimova, V. A., Sklovsky, D. E., Kamitakahara, W. A. and Fischer, J. E. 1998, Statics and dynamics of interlayer interactions in the dense high-pressure graphite compound LiC_2, *Phys. Rev. B* **57**, 5182-5190.

[34] Emery, N., Herold, C. and Lagrange, P. 2005, Structural study and crystal chemistry of the first stage calcium graphite intercalation compound, *J. Solid State Chem.* **178**, 2947-2952.

[35] Rakotomahevitra, A., Demangeat, C., Parlebas, J. C., Moraitis, G. and Razafindrakoto, E. 1992, Electronic-structure and properties of light-atoms intercalated in graphite, *J. Phys. Condens. Matter.* **4**, 4621-4632.

[36] Hartwigsen, C., Witschel, W. and Spohr, E. 1997, Charge density and charge transfer in stage-1 alkali-graphite intercalation compounds, *Phys. Rev. B* **55**, 4953-4959.

[37] Gonze, X., Beuken, J. M., Caracas, R., Detraux, F., Fuchs, M., Rignanese, G. M., Sindic, L., Verstraete, M., Zerah, G., Jollet, F., Torrent, M., Roy, A., Mikami, M., Ghosez, P., Raty, J. Y. and Allan, D. C. 2002, First-principles computation of material properties: the ABINIT software project, *Computational Materials Science* **25**, 478-492.

[38] http://opiumproject.sourceforge.net/.

[39] Perdew, J. P. and Wang, Y. 1992, Accurate and simple analytic representation of the electron-gas correlation energy, *Phys. Rev. B* **45**, 13244-13249.

[40] Ceperley, D. M. and Alder, B. J. 1980, Ground State of the Electron Gas by a Stochastic Method, *Phys. Rev. Lett.* **45**, 566-569.

[41] Imai, Y. and Watanabe, A. 2007, Energetic evaluation of possible stacking structures of Li-intercalation in graphite using a first-principle pseudopotential calculation, *J. Alloy. Comp.* **439**, 258-267.

[42] Guerarda, D. and Janot, R. 2004, Structure of the superdense LiC_3 compound prepared by ball-milling, *J. Phys. Chem. Solid.* **65**, 147-152.

[43] Broyden, C. 1970, The Convergence of a Class of Double-rank Minimization Algorithms: 2. The New Algorithm, *IMA.J.Appl.Math* **6**, 222-231.

[44] Fletcher, R. 1970, A new approach to variable metric algorithms, *Comput. J.* **13**, 317-322.

[45] Shanno, D. F. 1970, Conditioning of Quasi-Newton Methods for Function Minimization, *Math. Comput.* **24**, 647-656.

[46] Goldfarb, D. 1970, A family of variable-metric methods derived by variational means, *Math. Comput.* **24**, 23-&.

[47] Nicklow, R., Wakabayashi, N. and Smith, H. G. 1972, Lattice Dynamics of Pyrolytic Graphite, *Phys. Rev. B* **5**, 4951-4962.

[48] Nelmes, R. J., Loveday, J. S., Allan, D. R., Besson, J. M., Hamel, G., Grima, P. and Hull, S. 1993, Neutron- and x-ray-diffraction measurements of the bulk modulus of boron, *Phys. Rev. B* **47**, 7668-7673.

[49] Kganyago, K. R. and Ngoepe, P. E. 2003, Structural and electronic properties of lithium intercalated graphite LiC_6, *Phys. Rev. B* **68**, 205111.

[50] Bosak, A., Krisch, M., Mohr, M., Maultzsch, J. and Thomsen, C. 2007, Elasticity of single-crystalline graphite: Inelastic x-ray scattering study, *Phys. Rev. B* **75**, 153408.

[51] Ma, Y. 2007, Simulation of interstitial diffusion in graphite, *Phys. Rev. B* **76**, 075419.

[52] Tohei, T., Kuwabara, A., Oba, F. and Tanaka, I. 2006, Debye temperature and stiffness of carbon and boron nitride polymorphs from first principles calculations, *Phys. Rev. B* **73**, 064304.

[53] Rabii, S. and Guerard, D. 2008, Stability of superdense lithium graphite compounds, *J. Phys. Chem. Solid.* **69**, 1165-1167.

[54] Duan, J., Xue, R., Xu, Y. and Sun, C. 2008, Preparation of boron nitride flakes by a simple powder reaction, *J. Ceram. Soc. Japan* **116**, 354-356.

[55] Solozhenko, V. and Peun, T. 1997, Compression and thermal expansion of hexagonal graphite-like boron nitride up to 7 GPa and 1800 K, *J. Phys. Chem. Solid.* **58**, 1321-1323.

[56] Qi, Y. and Louis G. Hector, J. 2007, Planar stacking effect on elastic stability of hexagonal boron nitride, *Appl. Phys. Lett.* **90**, 081922.

[57] Chen, X., Cheng, Y., Xie, X., Feng, W. and Wu, K. 2007, Calculation of the ionic conductivity of h-BN and its effect on the dielectric loss, *J. Phys. Appl. Phys.* **40**, 846-849.

[58] Kobayashi, K., Watanabe, K. and Taniguchi, T. 2007, First-principles study of various hexagonal BN phases, *J. Phys. Soc. Jpn.* **76**.

[59] Barrett, C. S. 1956, X-ray study of the alkali metals at low temperatures, *Acta Crystallogr.* **9**, 671-677.

[60] Anderson, M. S. and Swenson, C. A. 1985, Experimental equations of state for cesium and lithium metals to 20 kbar and the high-pressure behavior of the alkali metals, *Phys. Rev. B* **31**, 668-680.

[61] Gshneider, K. A. 1964, *Solid State Phys.* **16**, 276.

[62] Boettger, J. C. and Trickey, S. B. 1985, Equation of state and properties of lithium, *Phys. Rev. B* **32**, 3391–3398.

[63] Khantha, M., Cordero, N. A., Molina, L. M., Alonso, J. A. and Girifalco, L. A. 2004, Interaction of lithium with graphene: An ab initio study, *Phys. Rev. B* **70**, 125422.

[64] Masago, A., Shirai, K. and Katayama-Yoshida, H. 2006, Crystal stability of α- and β-boron, *Phys. Rev. B* **73**, 104102.

[65] Shirai, K., Masago, A. and Katayama-Yoshida, H. 2007, High-pressure properties and phase diagram of boron, *Phys. Status Solidi B* **244**, 303-308.

[66] Widom, M. and Mihalkovic, M. 2008, Symmetry-broken crystal structure of elemental boron at low temperature, *Phys. Rev. B* **77**, 064113.

[67] Decker, B. F. and Kasper, J. S. 1959, The crystal structure of a simple rhombohedral form of boron, *Acta Crystallogr.* **12**, 503-506.

[68] Zoroddu, A., Bernardini, F., Ruggerone, P. and Fiorentini, V. 2001, First-principles prediction of structure, energetics, formation enthalpy, elastic constants, polarization, and piezoelectric constants of AlN, GaN, and InN: Comparison of local and gradient-corrected density-functional theory, *Phys. Rev. B* **64**, 045208.

[69] Fiorentini, V., Methfessel, M. and Scheffler, M. 1993, Electronic and structural properties of GaN by the full-potential linear muffin-tin orbitals method: The role of the d electrons, *Phys. Rev. B* **47**, 13353-13362.

[70] Mulliken, R. S. 1955, Electronic Population Analysis on LCAO-MO Molecular Wave Functions. I, *J. Chem. Phys.* **23**, 1833-1840.

[71] Löwdin, P.-O. 1950, On the Non-Orthogonality Problem Connected with the Use of Atomic Wave Functions in the Theory of Molecules and Crystals, *The Journal of Chemical Physics* **18**, 365-375.

[72] Hirshfeld, F. L. 1977, Spatial partitioning of charge-density, *Israel J. Chem.* **16**, 198-201.

[73] Bader, R. F. W., 1990, *Atoms in Molecules A Quantum Theory*, Oxford University Press.

[74] Chan, C. T., Kamitakahara, W. A., Ho, K. M. and Eklund, P. C. 1987, Charge-transfer effects in graphite intercalates: Ab initio calculations and neutron-diffraction experiment, *Phys. Rev. Lett.* **58**, 1528-1531.

[75] Pietronero, L. and Strässler, S. 1981, Bond-Length Change as a Tool to Determine Charge Transfer and Electron-Phonon Coupling in Graphite Intercalation Compounds, *Phys. Rev. Lett.* **47**, 593-596.

[76] Mansour, A. and Schnatterly, S. 1987, Electronic Structure of LiC_6 Studied by Soft X-Ray Emission Spectroscopy, *Physica Scripta.* **35**.

[77] Eberhardt, W., McGovern, I. T., Plummer, E. W. and Fisher, J. E. 1980, Charge-Transfer and Non-Rigid-Band Effects in the Graphite Compound LiC_6, *Phys. Rev. Lett.* **44**, 200-204.

[78] Hirshfeld, F. L. 1977, Charge deformation and vibrational smearing, *Israel J. Chem.* **16**, 168-174.

[79] Hirshfeld, F. L. 1977, Deformation density refinement program, *Israel J. Chem.* **16**, 226-229.

[80] Leenaerts, O., Partoens, B. and Peeters, F. M. 2008, Paramagnetic adsorbates on graphene: A charge transfer analysis, *Appl. Phys. Lett.* **92**, 243125.

[81] Gruneis, A., Pichler, T., Shiozawa, H., Attaccalite, C., Wirtz, L., Molodtsov, S. L., Follath, R., Weber, R. and Rubio, A. 2007, Low energy quasiparticle dispersion of graphite by angle-resolved photoemission spectroscopy, *Phys. Status Solidi B* **244**, 4129-4133.

[82] Gruneis, A., Attaccalite, C., Pichler, T., Zabolotnyy, V., Shiozawa, H., Molodtsov, S. L., Inosov, D., Koitzsch, A., Knupfer, M., Schiessling, J., Follath, R., Weber, R., Rudolf, P., Wirtz, L. and Rubio, A. 2008, Electron-Electron Correlation in Graphite: A Combined Angle-Resolved Photoemission and First-Principles Study, *Phys. Rev. Lett.* **100**, 037601.

[83] Leem, C. S., Kim, B. J., Kim, C., Park, S. R., Ohta, T., Bostwick, A., Rotenberg, E., Kim, H. D., Kim, M. K., Choi, H. J. and Kim, C. 2008, Effect of Linear Density of States on the Quasiparticle Dynamics and Small Electron-Phonon Coupling in Graphite, *Phys. Rev. Lett.* **100**, 016802.

[84] Sadowski, M. L., Martinez, G., Potemski, M., Berger, C. and de Heer, W. A. 2006, Landau Level Spectroscopy of Ultrathin Graphite Layers, *Phys. Rev. Lett.* **97**, 266405.

[85] Charlier, J.-C., Michenaud, J.-P., Gonze, X. and Vigneron, J.-P. 1991, Tight-binding model for the electronic properties of simple hexagonal graphite, *Phys. Rev. B* **44**, 13237-13249.

[86] Charlier, J.-C., Gonze, X. and Michenaud, J.-P. 1991, First-principles study of the electronic properties of graphite, *Phys. Rev. B* **43**, 4579-4589.

[87] Pivetta, M., Patthey, F., Barke, I., Hovel, H., Delley, B. and Schneider, W. D. 2005, Gap opening in the surface electronic structure of graphite induced by adsorption of alkali atoms: Photoemission experiments and density functional calculations, *Phys. Rev. B* **71**, 165430.

[88] Ooi, N., Rairkar, A. and Adams, J. B. 2006, Density functional study of graphite bulk and surface properties, *Carbon* **44**, 231-242.

[89] Arnaud, B., Lebegue, S., Rabiller, P. and Alouani, M. 2006, Huge Excitonic Effects in Layered Hexagonal Boron Nitride, *Phys. Rev. Lett.* **96**, 026402.

[90] Cappellini, G., Satta, G., Palummo, M. and Onida, G. 2001, Optical properties of BN in cubic and layered hexagonal phases, *Phys. Rev. B* **64**, 035104.

[91] Tarrio, C. and Schnatterly, S. E. 1989, Interband transitions, plasmons, and dispersion in hexagonal boron nitride, *Phys. Rev. B* **40**, 7852-7859.

[92] Giovannetti, G., Khomyakov, P. A., Brocks, G., Kelly, P. J. and van den Brink, J. 2007, Substrate-induced band gap in graphene on hexagonal boron nitride: Ab initio density functional calculations, *Phys. Rev. B* **76**, 073103.

[93] Watanabe, K., Taniguchi, T. and Kanda, H. 2004, Direct-bandgap properties and evidence for ultraviolet lasing of hexagonal boron nitride single crystal, *Nat. Mater.* **3**, 404-409.

[94] Blase, X., Rubio, A., Louie, S. G. and Cohen, M. L. 1995, Quasiparticle band structure of bulk hexagonal boron nitride and related systems, *Phys. Rev. B* **51**, 6868–6875.

[95] Mazin, I. I., Boeri, L., Dolgov, O. V., Golubov, A. A., Bachelet, G. B., Giantomassi, M. and Andersen, O. K. 2007, Unresolved problems in superconductivity of CaC_6, *Physica C-superconductivity Its Applications* **460**, 116-120.

[96] Csanyi, G., Littlewood, P. B., Nevidomskyy, A. H., Pickard, C. J. and Simons, B. D. 2005, The role of the interlayer state in the electronic structure of superconducting graphite intercalated compounds, *Nature Phys.* **1**, 42-45.

[97] Holzwarth, N. A. W., Rabii, S. and Girifalco, L. A. 1978, Theoretical study of lithium graphite. I. Band structure, density of states, and Fermi-surface properties, *Phys. Rev. B* **18**, 5190-5205.

[98] Holzwarth, N. A. W., Girifalco, L. A. and Rabii, S. 1978, Theoretical study of lithium graphite. II. Spatial distribution of valence electrons, *Phys. Rev. B* **18**, 5206-5216.

[99] Delhaes, P. , Rouillon, J.C. , Manceau, J.P. , Guerard, D. and Herold, A. 1976, Paramagnetism and specific heat of the graphite lamellar compound C6Li, *J. Phys. Lattr.* **37**, 127-129.

[100] Ahuja, R., Auluck, S., Wills, J. M., Alouani, M., Johansson, B. and Eriksson, O. 1997, Optical properties of graphite from first-principles calculations, *Phys. Rev. B* **55**, 4999-5005.

[101] Ahuja, R., Auluck, S., Eriksson, O. and Johansson, B. 1997, Calculated electronic and optical properties of a graphite intercalation compound: LiC_6, *J. Phys.: Condens. Matter* **9**, 9845-9852.

[102] Law, A. R., Barry, J. J. and Hughes, H. P. 1983, Angle-resolved photoemission and secondary electron emission from single-crystal graphite, *Phys. Rev. B* **28**, 5332-5335.

[103] Bianconi, A., Hagström, S. B. M. and Bachrach, R. Z. 1977, Photoemission studies of graphite high-energy conduction-band and valence-band states using soft-x-ray synchrotron radiation excitation, *Phys. Rev. B* **16**, 5543-5548.

[104] Blase, X., Rubio, A., Louie, S. G. and Cohen, M. L. 1994, Stability and Band Gap Constancy of Boron Nitride Nanotubes, *Europhys. Lett.* **28**.

[105] Margine, E. R. and Crespi, H. C. 2006, Universal Behavior of Nearly Free Electron States in Carbon Nanotubes, *Phys. Rev. Lett.* **96**.

[106] Pacilé, D., Papagno, M., Rodríguez, A. F., Grioni, M., Papagno, L., Ç. Ö. Girit, Meyer, J. C., Begtrup, G. E. and Zettl, A. 2008, Near-Edge X-Ray Absorption Fine-Structure Investigation of Graphene, *Physical Review Letters* **101**, 066806.

[107] Calandra, M. and Mauri, F. 2005, Theoretical Explanation of Superconductivity in C_6Ca, *Phys. Rev. Lett.* **95**, 237002.

[108] Sugawara, K., Sato, T. and Takahashi, T. 2009, Fermi-surface-dependent superconducting gap in C_6Ca, *Nat. Phys.* **5**.

[109] Reich, S. and Thomsen, C. 2004, Raman spectroscopy of graphite, *Philosophical Transactions of the Royal Society of London. Series A: Mathematical, Physical and Engineering Sciences* **362**, 2271-2288.

[110] Mohr, M., Maultzsch, J., Dobardžić, E., Reich, S., Milošević, I., Damnjanović, M., Bosak, A., Krisch, M. and Thomsen, C. 2007, Phonon dispersion of graphite by inelastic x-ray scattering, *Physical Review B (Condensed Matter and Materials Physics)* **76**, 035439.

[111] Maultzsch, J., Reich, S., Thomsen, C., Requardt, H. and Ordejón, P. 2004, Phonon Dispersion in Graphite, *Phys. Rev. Lett.* **92**, 075501.

[112] Zabel, H., Magerl, A. and Rush, J. J. 1983, Phonons in LiC6, *Phys. Rev. B* **27**, 3930-3933.

[113] Piscanec, S., Lazzeri, M., Mauri, F., Ferrari, A. C. and Robertson, J. 2004, Kohn Anomalies and Electron-Phonon Interactions in Graphite, *Phys. Rev. Lett.* **93**, 185503.

[114] Sánchez-Portal, D., Artacho, E., Soler, J. M., Rubio, A. and Ordejón, P. 1999, Ab initio structural, elastic, and vibrational properties of carbon nanotubes, *Phys. Rev. B* **59**, 12678–12688.

[115] Dubay, O. and Kresse, G. 2003, Accurate density functional calculations for the phonon dispersion relations of graphite layer and carbon nanotubes, *Phys. Rev. B* **67**, 035401.

[116] Mounet, N. and Marzari, N. 2005, First-principles determination of the structural, vibrational and thermodynamic properties of diamond, graphite, and derivatives, *Phys. Rev. B* **71**, 205214.

[117] Lang, L., Doyen-Lang, S., Charlier, A. and Charlier, M. F. 1994, Dynamical study of graphite and graphite intercalation compounds, *Phys. Rev. B* **49**, 5672–5681.

[118] Blakslee, O. L., Proctor, D. G., Seldin, E. J., Spence, G. B. and Weng, T. 1970, Elastic Constants of Compression-Annealed Pyrolytic Graphite, *J. Appl. Phys.* **41**, 3373-3382.

[119] Seldin, E. J. and Nezbeda, C. W. 1970, Elastic Constants and Electron-Microscope Observations of Neutron-Irradiated Compression-Annealed Pyrolytic and Single-Crystal Graphite, *Journal of Applied Physics* **41**, 3389-3400.

[120] Reich, S., Ferrari, A. C., Arenal, R., Loiseau, A., Bello, I. and Robertson, J. 2005, Resonant Raman scattering in cubic and hexagonal boron nitride, *Phys. Rev. B* **71**, 205201.

[121] Nemanich, R. J., Solin, S. A. and Martin, R. M. 1981, Light scattering study of boron nitride microcrystals, *Phys. Rev. B* **23**, 6348–6356.

[122] Geick, R., Perry, C. H. and Rupprecht, G. 1966, Normal Modes in Hexagonal Boron Nitride, *Phys. Rev.* **146**, 543–547.

[123] Serrano, J., Bosak, A., Arenal, R., Krisch, M., Watanabe, K., Taniguchi, T., Kanda, H., Rubio, A. and Wirtz, L. 2007, Vibrational Properties of Hexagonal Boron Nitride: Inelastic X-Ray Scattering and Ab Initio Calculations, *Physical Review Letters* **98**, 095503.

[124] Boeri, L., Bachelet, G. B., Giantomassi, M. and Andersen, O. K. 2007, Electron-phonon interaction in graphite intercalation compounds, *Phys. Rev. B* **76**, 064510.

[125] Emery, N., Hérold, C., d'Astuto, M., Garcia, V., Bellin, C., Marêché, J. F., Lagrange, P. and Loupias, G. 2005, Superconductivity of Bulk CaC_6, *Phys. Rev. Lett.* **95**, 087003.

[126] Calandra, M. and Mauri, F. 2006, Possibility of superconductivity in graphite intercalated with alkaline earths investigated with density functional theory, *Physical Review B (Condensed Matter and Materials Physics)* **74**, 094507.

[127] Bosak, A., Serrano, J., Krisch, M., Watanabe, K., Taniguchi, T. and Kanda, H. 2006, Elasticity of hexagonal boron nitride: Inelastic x-ray scattering measurements, *Physical Review B (Condensed Matter and Materials Physics)* **73**, 041402.

[128] Ohba, N., Miwa, K., Nagasako, N. and Fukumoto, A. 2001, First-principles study on structural, dielectric, and dynamical properties for three BN polytypes, *Phys. Rev. B* **63**, 115207.

[129] Green, J. F., Bolland, T. K. and Bolland, J. W. 1976, Theoretical elastic behavior for hexagonal boron nitride, *The Journal of Chemical Physics* **64**, 656-662.

[130] Boettger, J. C. 1997, All-electron full-potential calculation of the electronic band structure, elastic constants, and equation of state for graphite, *Phys. Rev. B* **55**, 11202–11211.

CURRICULUM VITAE

Bahadır Altıntaş

Address:

Abant İzzet Baysal University
Department of Chemistry,
Gölköy-Bolu, Turkey
Phone: +90 374 2541000
Fax: +90 374 2534642
Email: *bahadir.altintas@gmail.com*

Personal Details:

Gender: Male
Date of birth: 6^{th} of September, 1977
Place of birth: Ankara, Turkey

Education:

1995-2000 Undergraduate Studies in Chemistry at Abant Izzet Baysal University

2000-2003 MSc in Chemistry at Abant Izzet Baysal University
Thesis: Investigation Of The Photochemical Ketone Coordination To Tungsten Hexacarbonyl.

2003-2009 PhD in Chemistry at the Abant Izzet Baysal University
Thesis: Ab initio investigations on electronic and lattice dynamical properties of intercalation of metals into hexagonal boron nitride.

Specialization: Inorganic Chemistry, Computational Chemistry.

Publications:

1. Altintas B., Bozkurt C. "A comparative study on aldol-type condensation reactions of cyclic, acyclic and substituted cyclic ketones by the $W(CO)_6/CCl_4$/UV system , Applied Organometallic Chemistry, vol.19,12,1220-1224,2005

Presentations:

1. First principles investigations into alkali intercalation of hexagonal boron nitride American Physical Society March Meeting, New Orleans-Louisiana (2008)(Oral Presentation).

2. Ab-initio investigations on electronic and lattice dynamical properties on intercalation of Cu (copper) into hexagonal boron nitride(hBN). American Physical Society March Meeting, Denver-Colorado (2007) (Oral Presentation).

3. First principles investigation of Cu(Copper) intercalation in hexagonal boron nitride(hBN) XX. National Chemistry Congress, Kayseri-Turkey (2006)(Poster).

4. The Effect of Transition Metals on The Structure of h-BN Intercalation Compounds I. National Boron Workshop , Ankara-Turkey (2005)(Poster).

5. Photochemical ketone coordination to tungsten hexacarbonyl" XVIII. National Chemistry Congress, Kars-Turkey (2004)(Poster).

Working Experience:

2000-2009 Working in Abant Izzet Baysal University, Chemistry Department as a research assistant.